# Cyclic viscoelastoplasticity of polypropylene/nanoclay composites

Drozdov, A.; Christiansen, Jesper de Claville

*Published in:*
Mechanics of Time Dependent Materials

*DOI (link to publication from Publisher):*
10.1007/s11043-012-9169-x

*Publication date:*
2012

*Document Version*
Early version, also known as pre-print

# *Cyclic viscoelastoplasticity of polypropylene/nanoclay composites*

**A. D. Drozdov & J. deC. Christiansen**

**Mechanics of Time-Dependent Materials**
An International Journal Devoted to the Time-Dependent Behaviour of Materials and Structures

ISSN 1385-2000

Mech Time-Depend Mater
DOI 10.1007/s11043-012-9169-x

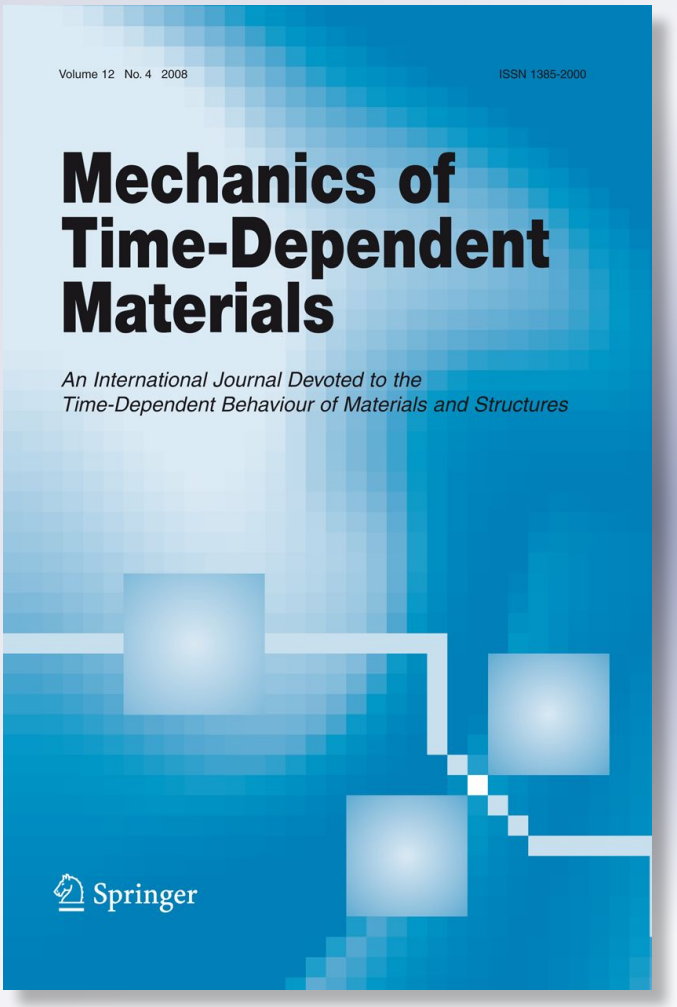


Springer

Mech Time-Depend Mater
DOI 10.1007/s11043-012-9169-x

# Cyclic viscoelastoplasticity of polypropylene/nanoclay composites

**A.D. Drozdov · J. deC. Christiansen**

Received: 5 April 2011 / Accepted: 23 December 2011


**Abstract** Observations are reported on isotactic polypropylene/organically modified nanoclay hybrids with concentrations of filler ranging from 0 to 5 wt.% in cyclic tensile tests with a stress–controlled program (oscillations between various maximum stresses and the zero minimum stress). A pronounced effect of nanofiller is demonstrated: reinforcement with 2 wt.% of clay results in strong reduction of maximum and minimum strains per cycle and growth of number of cycles to failure compared with neat polypropylene. To rationalize these findings, a constitutive model is developed in cyclic viscoelasticity and viscoplasticity of polymer nanocomposites. Adjustable parameters in the stress–strain relations are found by fitting experimental data. The model correctly describes the growth of the ratcheting strain and shows that fatigue failure is driven by a pronounced increase in plastic strain in the crystalline phase. To assess the influence of loading conditions on the changes in the material parameters, experimental data on polypropylene are studied in cyclic tests with a strain–controlled program (oscillations between fixed maximum and minimum strains) and a mixed program (oscillations between various maximum strains and the zero minimum stress). Numerical simulation confirms the ability of the model to predict the evolution of stress–strain diagrams with the number of cycles.

**Keywords** Polymer nanocomposite · Viscoelasticity · Viscoplasticity · Cyclic deformation · Constitutive modeling

## 1 Introduction

This paper is concerned with experimental investigation and constitutive modeling of the mechanical response of polymer/clay nanocomposites in uniaxial tensile cyclic tests with a

A.D. Drozdov (✉)
Department of Plastics Technology, Danish Technological Institute, Gregersensvej 1, Taastrup 2630, Denmark
e-mail: Aleksey.Drozdov@teknologisk.dk

J. deC. Christiansen
Department of Mechanical and Manufacturing Engineering, Aalborg University, Fibigerstraede 16, Aalborg 9220, Denmark

Published online: 07 March 2012

stress-controlled program (ratcheting between various maximum stresses $\sigma^{\max}$ and the zero minimum stress $\sigma^{\min}$).

A number of studies revealed noticeable improvement of viscoelastic and viscoplastic properties of polymers due to their reinforcement with nanoclay (Tjong 2006; Pavlidou and Papaspyrides 2008). This enhancement remained, however, rather modest compared with what has been expected from the effect of reinforcement about a decade ago (Cotterell et al. 2007; Jancar et al. 2010). Several hypotheses have been suggested to explain this inconsistency: (i) inhomogeneity in the distribution of nanoparticles driven by clustering of clay platelets and insufficient intercalation and exfoliation of stacks (Luo and Daniel 2003), (ii) the presence of inter-inclusion interactions reducing stiffness of nanocomposites and resulting in formation of a hierarchical structure of filler particles (Zeng et al. 2008), (iii) weak adhesion between polymer chains and clay particles with high aspect ratios (Fu et al. 2008) that causes a significant embrittlement of hybrids (Cotterell et al. 2007), (iv) development of interphase zones around stacks of clay platelets with strongly reduced mobility of chains (Qiao and Brinson 2009), etc.

Keeping in mind discrepancies between expected and real mechanical properties of nanohybrids, it seems natural to concentrate on more sophisticated (compared with uniaxial tension) loading programs, where the effect of nanofiller becomes significant for engineering applications. The latter approach was initiated by Yang et al. (2006), Lietz et al. (2007), Drozdov et al. (2009), who demonstrated that reinforcement of polymers with nanoparticles dramatically enhanced creep resistance. Wang and Zhao (2008a, 2008b) showed that ratcheting strain in cyclic tests with a stress-controlled program was substantially reduced due to the presence of nanoparticles.

The objective of this study is three-fold:

1. To report observations in uniaxial tensile cyclic tests with a stress-controlled program on polypropylene/clay hybrids with various concentrations of filler and to demonstrate that the presence of nanoclay induces a strong decrease in maximum and minimum strains per cycle and growth of number of cycles to failure.
2. To develop constitutive equations in cyclic viscoelasticity and viscoplasticity of polymer nanocomposites and to find adjustable parameters in the stress–strain relations by fitting the observations.
3. To demonstrate ability of the model to predict the mechanical response in cyclic tests with different deformation programs (stress-controlled, strain-controlled, and mixed) and to examine the effect of loading conditions on evolution of materials parameters.

A number of studies dealt in the past five years with the viscoelastoplastic behavior of polymers and polymer composites subjected to cyclic loading (Drozdov and Christiansen 2007; Yakimets et al. 2007; Sullivan 2008; Drozdov 2009; Mizuno and Sanomura 2009; Ayoub et al. 2010; Bouchart et al. 2010). The stress–strain relations developed in those works were confined, however, to the description of the first cycle of loading–unloading and could not be applied directly to fitting observations in multi-cycle tests. The first attempts to predict the response of polymers subjected to severe (hundreds of cycles) cyclic deformations were undertaken by Ayoub et al. (2011) and Drozdov (2011).

Constitutive models in viscoplasticity of crystalline materials (where the viscoelastic phenomena are of secondary importance) under cyclic loading with stress-controlled programs were critically evaluated by Bari and Hassan (2002), Chaboche (2008), Kang (2008), and Sai (2011). It was pointed out that the governing equations captured some characteristic features of observations on metals, but (i) their ability to predict evolution of ratcheting strain was far from being satisfactory, and (ii) they failed to predict the mechanical response

under loading with one program when material parameters are found by fitting stress–strain diagrams under deformation with another program.

To develop a model for the mechanical behavior polymer/clay nanocomposites that involves a reasonable number of adjustable parameters, a two-step approach is proposed. At the first step, stress–strain relations are derived for an individual cycle of loading–retraction. These relations contain several material parameters that are treated as constants. At the other step, these parameters are allowed to change slowly with number of cycles, and kinetic equations for their evolution are introduced. Coefficients in the kinetic equations are found by fitting observations along the first several cycles of loading–retraction. Validity of these relations is confirmed by comparing predictions of the model with observations in cyclic tests where number of cycles strongly exceeds that used for determination of material constants.

The exposition is organized as follows. Observations in uniaxial tensile cyclic tests with stress-controlled deformation program are reported in Sect. 2. Stress–strain relations for the viscoelastic and viscoplastic responses of polymer nanocomposites under tensile cyclic deformation are presented in Sect. 3 (derivation of constitutive equations for an arbitrary three-dimensional deformation with small strains is given in the Appendix). Adjustable parameters in the governing equations are determined in Sect. 4 by fitting the experimental data. Experimental investigation and modeling of cyclic deformations of polypropylene with mixed and strain-controlled programs is performed in Sects. 5 and 6, respectively. Concluding remarks are formulated in Sect. 7.

## 2 Experimental results

Isotactic polypropylene Moplen HP 400R (density 0.90 g/cm$^3$, melt flow rate 25 g/10 min, melting temperature 161°C) was purchased from Albis Plastic Scandinavia AB (Sweden). Maleic anhydride grafted polypropylene Eastman G 3015 (acid number 15 mg KOH/g) was supplied by Eastman Chemical Company (USA). Organically modified montmorillonite nanoclay Delitte 67G was donated by Laviosa Chimica Mineraria S.p.A. (Italy).

Hybrid nanocomposites were manufactured in a two-step process (Drozdov et al. 2009). At the first step, a masterbatch was prepared in a twin-screw extruder Brabender PL2000 with processing temperature 200°C, screw speed 200 rpm, and throughput 5 kg/h. The masterbatch contained 40 wt.% of polypropylene, 40 wt.% of maleic anhydride grafted polypropylene, and 20 wt.% of nanoclay (clay/compatibilizer proportion 1:2). Prior to extrusion, all components were dried in an oven at 80°C overnight. At the other step, pellets of the masterbatch were mixed with polypropylene in various proportions corresponding to nanoclay concentrations $\chi = 0$, 2, and 5 wt.%. Dumbbell specimens for tensile tests (ASTM standard D638) with cross-sectional area 10.2 mm$\times$4.2 mm were molded by using injection-molding machine Arburg 320C.

Mechanical tests were performed by means of universal testing machine Instron–5569 equipped with an electro-mechanical sensor for control of longitudinal strains. The tensile force was measured by a 5 kN load cell. The engineering stress $\sigma$ was determined as the ratio of axial force to cross-sectional area of undeformed specimens.

Two series of uniaxial tensile tests were conducted at room temperature.

The first series involved five ratcheting tests with various maximum stresses $\sigma^{\max}$, minimum stress $\sigma^{\min} = 1$ MPa, and cross-head speed $\dot{d} = 100$ mm/min (that corresponded to strain rate $\dot{\epsilon} = 1.7 \cdot 10^{-2}$ s$^{-1}$). A specimen was stretched with cross-head speed $\dot{d}$ up to maximum stress $\sigma^{\max}$, retracted down to minimum stress $\sigma^{\min}$ with the same cross-head speed, reloaded up to maximum stress $\sigma^{\max}$ with cross-head speed $\dot{d}$, unloaded down to

minimum stress $\sigma^{\min}$ with the same cross-head speed, etc. The tests involved 200 cycles of loading–retraction (some of them were terminated earlier due to breakage of specimens). Each test was carried out on a new sample and repeated by twice to confirm reproducibility of measurements.

The minimum stress $\sigma^{\min} = 1$ MPa was chosen instead of $\sigma^{\min} = 0$ to avoid buckling of samples. The cross-head speed $\dot{d} = 100$ mm/min was selected to ensure that maximum duration of cyclic tests did not exceed 20 min (the conventional duration of short-term creep and relaxation tests).

Ratcheting tests on neat polypropylene ($\chi = 0$) were performed with maximum strains $\sigma^{\max} = 24$, 26, 28, 30, and 32 MPa. Tests on polypropylene/clay nanocomposites were carried out with maximum stresses $\sigma^{\max} = 28$, 30, 32, 34, and 35 MPa ($\chi = 2$ wt.%) and $\sigma^{\max} = 28$, 30, 32, 33, and 34 MPa ($\chi = 5$ wt.%). For each clay content $\chi$, the highest maximum stress $\sigma^{\max}$ was chosen from the condition that fatigue failure occurred after at least 40 cycles of oscillations.

Experimental data in this series of tests are depicted in Figs. 1, 2 and 3, where maximum $\epsilon^{\max}$ and minimum $\epsilon^{\min}$ strains per cycle are plotted versus number of cycles $n$. The following conclusions are drawn from these figures:

1. Experimental diagrams $\epsilon^{\max}(n)$ and $\epsilon^{\min}(n)$ may be split into three intervals. Along the first (primary fatigue), the curves $\epsilon^{\max}(n)$ and $\epsilon^{\min}(n)$ are convex. Along the other interval (secondary fatigue), $\epsilon^{\max}$ and $\epsilon^{\min}$ grow linearly with $n$. At the last interval (tertiary fatigue), the dependencies $\epsilon^{\max}(n)$ and $\epsilon^{\min}(n)$ are nonlinear and concave.
2. Maximum and minimum strains strongly increase with $\sigma^{\max}$. For neat polypropylene ($\chi = 0$), maximum strain $\epsilon^{\max}$ after 200 cycles equals 0.030 at $\sigma^{\max} = 24$, 0.036 at $\sigma^{\max} = 26$, 0.059 at $\sigma^{\max} = 28$, and 0.115 at $\sigma^{\max} = 30$ MPa.
3. Reinforcement of polypropylene with nanoclay results in substantial reduction in maximum $\epsilon^{\max}$ and minimum $\epsilon^{\min}$ strains. After 200 cycles of loading–retraction with $\sigma^{\max} = 30$ MPa, maximum strain equals 0.115 at $\chi = 0$, 0.038 at $\chi = 2$, and 0.040 at $\chi = 5$ wt.%.
4. The most pronounced improvement of fatigue resistance is reached when concentration of filler equals 2 wt.%. This result is in accord with our previous studies on the same

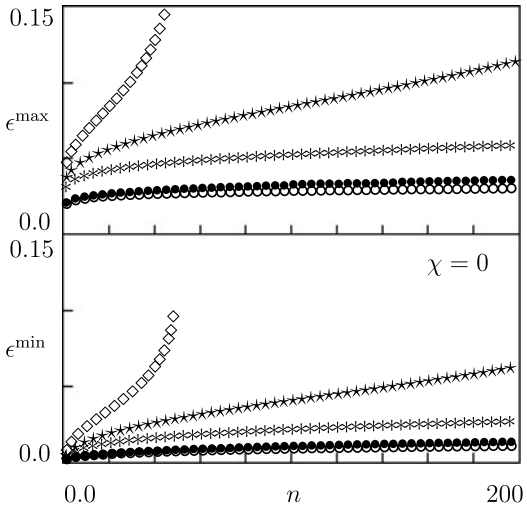


**Fig. 1** Maximum $\epsilon^{\max}$ and minimum $\epsilon^{\min}$ strains versus number of cycles $n$. *Symbols*: observations on nanocomposite with $\chi = 0$ wt.% of clay in cyclic tests with various maximum stresses $\sigma^{\max}$ MPa and minimum stress $\sigma^{\min} = 1$ MPa ($\diamond$ $\sigma^{\max} = 32$; $\star$ $\sigma^{\max} = 30$; $*$ $\sigma^{\max} = 28$; $\bullet$ $\sigma^{\max} = 26$; $\circ$ $\sigma^{\max} = 24$)

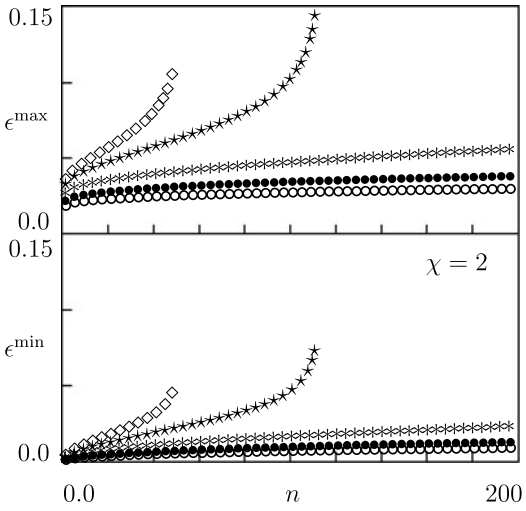


**Fig. 2** Maximum $\epsilon^{max}$ and minimum $\epsilon^{min}$ strains versus number of cycles $n$. *Symbols*: observations on nanocomposite with $\chi = 2$ wt.% of clay in cyclic tests with various maximum stresses $\sigma^{max}$ MPa and minimum stress $\sigma^{min} = 1$ MPa ($\diamond$ $\sigma^{max} = 35$; $\star$ $\sigma^{max} = 34$; $*$ $\sigma^{max} = 32$; $\bullet$ $\sigma^{max} = 30$; $\circ$ $\sigma^{max} = 28$)

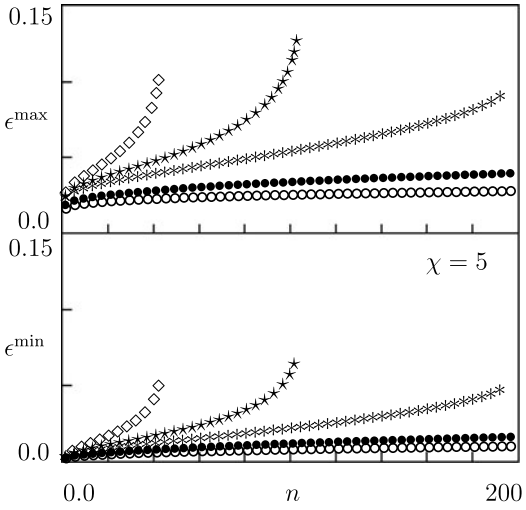


**Fig. 3** Maximum $\epsilon^{max}$ and minimum $\epsilon^{min}$ strains versus number of cycles $n$. *Symbols*: observations on nanocomposite with $\chi = 5$ wt.% of clay in cyclic tests with various maximum stresses $\sigma^{max}$ MPa and minimum stress $\sigma^{min} = 1$ MPa ($\diamond$ $\sigma^{max} = 34$; $\star$ $\sigma^{max} = 33$; $*$ $\sigma^{max} = 32$; $\bullet$ $\sigma^{max} = 30$; $\circ$ $\sigma^{max} = 28$)

polymer/clay hybrid (Drozdov et al. 2009), which demonstrated that nanocomposites with clay content of 1 to 2 wt.% had the highest resistance to creep flow.

The fact that some critical concentration $\chi_{cr}$ exists (such that enhancement of mechanical properties of nanohybrids is observed at $\chi < \chi_{cr}$ only) has been reported by several authors (Hsieh et al. 2004; Bikiaris et al. 2006). It is explained by (i) formation of a stable filler network structure in polymer nanocomposites (Wang et al. 2006; Su et al. 2011), (ii) development of constrained regions where mobility of chains is severely restricted by surrounding clay platelets and their stacks (Zhang and Loo 2009), and (iii) overlapping of interfacial layers of neighboring nanoparticles (Mortezaei et al. 2011).

In the other series of experiments, ratcheting tests were conducted with cross-head 100 mm/min, minimum stress $\sigma^{min} = 1$ MPa, and various maximum stresses $\sigma^{max}$ up to breakage of specimens. This series involved eight tests on neat polypropylene, three tests on nanocomposite with $\chi = 2$ wt.%, and 5 tests on polymer/clay hybrid with $\chi = 5$ wt.%. Observations

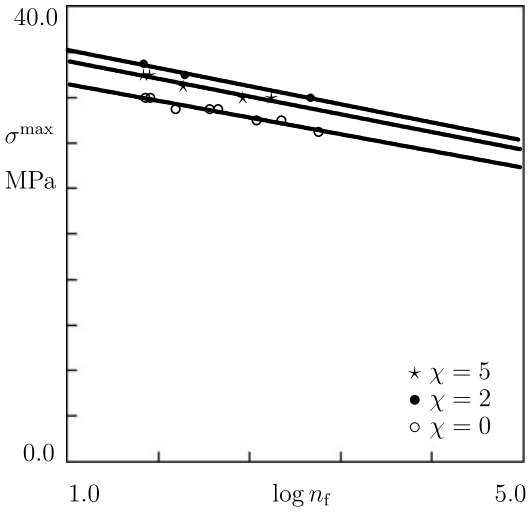


**Fig. 4** Maximum stress per cycle $\sigma^{\max}$ versus number of cycles to failure $n_f$. *Symbols*: observations on nanocomposites with various clay contents $\chi$ wt.% in cyclic tests with $\sigma^{\min} = 1$ MPa. *Solid lines*: approximation of the data by (1)

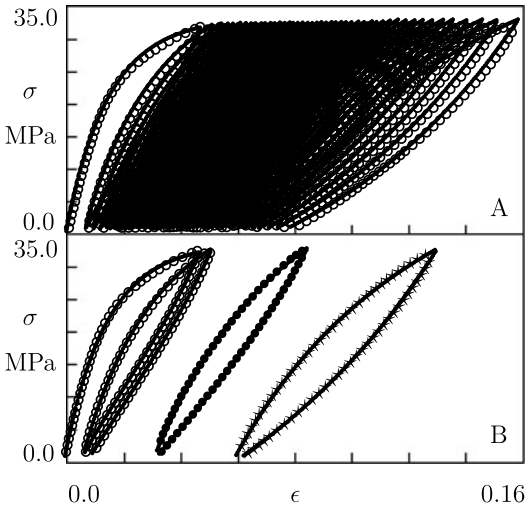


**Fig. 5** Stress $\sigma$ versus strain $\epsilon$. *Symbols*: observations on nanocomposite with $\chi = 0$ wt.% in the cyclic test with $\sigma^{\max} = 32$ MPa and $\sigma^{\min} = 1$ MPa. *Solid lines*: results of numerical simulation. **A**: 46 cycles of loading–retraction. **B**: selected cycles $\circ$ $n = 1, 2$; $\bullet$ $n = 20$; $\star$ $n = 40$

are depicted in Fig. 4 where maximum stress $\sigma^{\max}$ is plotted versus number of cycles to failure $n_f$. Following common practice, the semi-logarithmic plot is used with $\log = \log_{10}$. For each nanoclay content $\chi$, experimental data are approximated by the Eyring formula

$$\sigma^{\max} = \sigma_0 - \sigma_1 \log n_f, \tag{1}$$

where $\sigma_0$ and $\sigma_1$ are calculated by the least-squares method. Fig. 4 demonstrates that

1. Equation (1) adequately describes the data, while $\sigma_1$ is weakly affected by concentration of nanoclay.
2. Reinforcement of polypropylene causes strong (by two orders of magnitude) growth of number of cycles to failure.
3. The most pronounced enhancement of fatigue resistance is reached when clay content equals 2 wt.%.

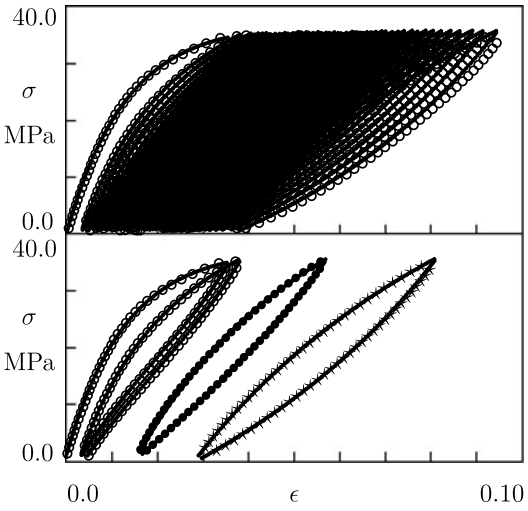


**Fig. 6** Stress $\sigma$ versus strain $\epsilon$. *Symbols*: observations on nanocomposite with $\chi = 2$ wt.% in the cyclic test with $\sigma^{\max} = 35$ MPa and $\sigma^{\min} = 1$ MPa. *Solid lines*: results of numerical simulation. **A**: 46 cycles of loading–retraction. **B**: selected cycles $\circ$ $n = 1, 2$; $\bullet$ $n = 20$; $\star$ $n = 40$

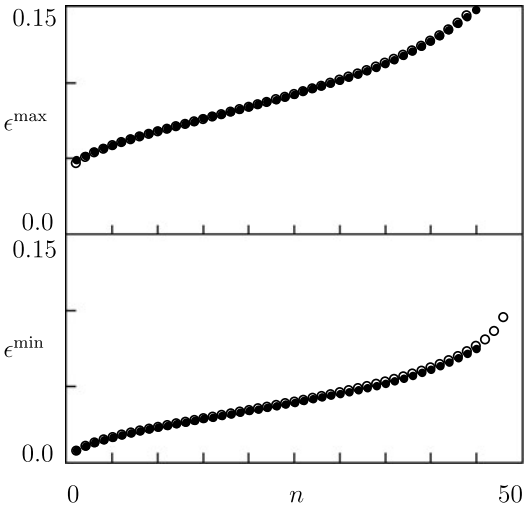


**Fig. 7** Maximum $\epsilon^{\max}$ and minimum $\epsilon^{\min}$ strains versus number of cycles $n$. *Unfilled circles*: observations on nanocomposite with $\chi = 0$ wt.% in the cyclic test with $\sigma^{\max} = 32$ MPa and $\sigma^{\min} = 1$ MPa. *Filled circles*: predictions of the model

Based on these observations, we confine ourselves to study of the mechanical response of nanocomposites with $\chi = 0$ and 2 wt.% only. Experimental stress–strain diagrams for these nanohybrids under cyclic loading with the highest maximum stresses ($\sigma^{\max} = 32$ MPa at $\chi = 0$ wt.% and $\sigma^{\max} = 35$ MPa at $\chi = 2$ wt.%) are depicted in Figs. 5 and 6, and corresponding dependencies of maximum and minimum strains on $n$ are plotted in Figs. 7 and 8. The data are chosen for the detailed analysis as the number of cycles to failure in ratcheting tests practically coincide. The following conclusions are drawn from Figs. 5, 6, 7 and 8:

1. The stress–strain curves under loading and unloading are strongly nonlinear.
2. An increase in number of cycles $n$ results in growth of hysteresis energy (calculated as the area between subsequent loading and unloading paths) and clockwise rotation of stress–strain diagrams.

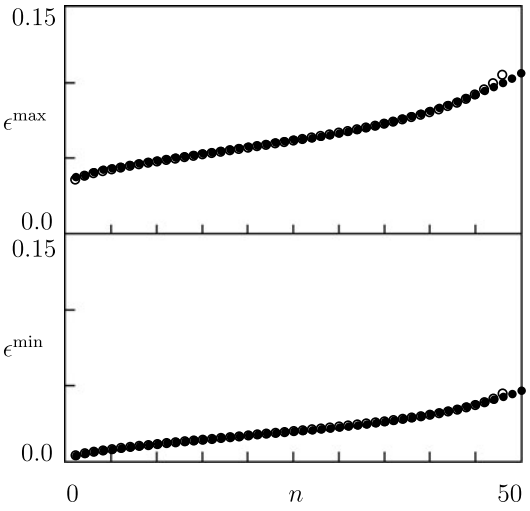


**Fig. 8** Maximum $\epsilon^{\max}$ and minimum $\epsilon^{\min}$ strains versus number of cycles $n$. *Unfilled circles*: observations on nanocomposite with $\chi = 2$ wt.% in the cyclic test with $\sigma^{\max} = 35$ MPa and $\sigma^{\min} = 1$ MPa. *Filled circles*: predictions of the model

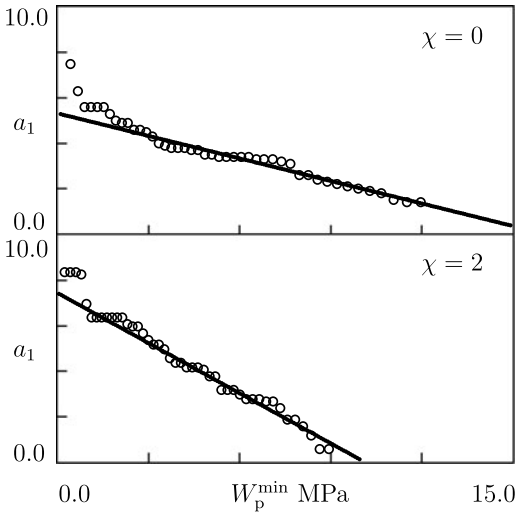


**Fig. 9** Parameter $a_1$ versus plastic work $W_{\mathrm{p}}^{\min}$. *Circles*: treatment of observations in cyclic tests on nanocomposites with various clay contents $\chi$ wt.%. *Solid lines*: approximation of the data by (9)

3. Reinforcement of polypropylene with nanoclay induces a strong decay in maximum strain per cycle: after 46 cycles of oscillations, $\epsilon^{\max}$ equals 0.158 at $\chi = 0$ wt.%, $\sigma^{\max} = 32$ MPa versus 0.096 at $\chi = 2$ wt.%, $\sigma^{\max} = 35$ MPa and 0.040 at $\chi = 2$ wt.%, $\sigma^{\max} = 32$ MPa.
4. Although fatigue failure of specimens with $\chi = 0$ and 2 wt.% occurs after the same number of cycles ($n_{\mathrm{f}} = 48$), maximum $\epsilon^{\max}$ and minimum $\epsilon^{\min}$ strains in ratcheting tests on nanocomposite with $\chi = 2$ wt.% are noticeably lower than those measured on neat polypropylene.

Experimental data reveal good reproducibility of measurements: maximum deviation between strains measured on different specimens under the same loading conditions does not exceed 6%.

## 3 Constitutive model

To rationalize these observations, constitutive equations are derived for the viscoelastic and viscoplastic responses of nanocomposites under cyclic deformation. A two-step approach is employed for modeling. At the first step, stress–strain relations are developed in cyclic viscoelastoplasticity. These relations involve several adjustable parameters that are treated as constants for an individual cycle of loading–unloading. At the other step, kinetic equations are suggested for evolution of these quantities with number of cycles. Coefficients in the kinetic equations are found by fitting experimental data along the first several cycles (30 to 50) of loading–retraction. Validation of these equations is performed by comparison of the model predictions with observations in cyclic tests with relatively large numbers of cycles (that strongly exceed the number of cycles used to determine material constants).

### 3.1 Stress–strain relations

Constitutive equations in viscoelasticity and viscoplasticity of polymer nanocomposites under an arbitrary three-dimensional deformation with small strains are developed in the Appendix. We present a simplified version of these relations for uniaxial tensile cyclic loading with constant strain rate $\dot{\epsilon}$.

Strain $\epsilon$ equals the sum of elastic $\epsilon_e$ and plastic $\epsilon_p$ strains

$$\epsilon = \epsilon_e + \epsilon_p. \tag{2}$$

The plastic strain $\epsilon_p$ is split into the sum of two components

$$\epsilon_p = \epsilon_{p1} + \epsilon_{p2} \tag{3}$$

that reflect plastic deformation in the crystalline and amorphous phases, respectively. The strain rate for plastic deformation in the crystalline phase is proportional to that for macrodeformation

$$\frac{d\epsilon_{p1}}{dt} = \phi\dot{\epsilon} \quad \text{(loading)}, \qquad \frac{d\epsilon_{p1}}{dt} = -\phi\dot{\epsilon} \quad \text{(unloading)}. \tag{4}$$

The coefficient $\phi$ obeys the differential equations

$$\frac{d\phi}{dt} = a_1\dot{\epsilon}(1-\phi)^2 \quad \text{(loading)}, \qquad \frac{d\phi}{dt} = -a_2\dot{\epsilon}(1-\phi)^2 \quad \text{(unloading)}, \tag{5}$$

where $a_1$ and $a_2$ are non-negative coefficients. The strain rate for plastic deformation in the amorphous matrix is governed by the equations

$$\begin{aligned} \frac{d\epsilon_{p2}}{dt} &= S_1\dot{\epsilon}\left[\epsilon_e(t) - R_1\epsilon_{p2}(t) - \int_0^\infty f(v)Z(t,v)dv\right] \quad \text{(loading)}, \\ \frac{d\epsilon_{p2}}{dt} &= S_2\dot{\epsilon}\left[\epsilon_e(t) - R_2\epsilon_{p2}(t) - \int_0^\infty f(v)Z(t,v)dv\right] \quad \text{(unloading)}, \end{aligned} \tag{6}$$

where $R_1$, $R_2$, $S_1$, and $S_2$ are non-negative parameters. The function $f(v)$ is determined by (A.7). The function $Z(t,v)$ obeys the differential equation

$$\frac{\partial Z}{\partial t}(t,v) = \Gamma(v)\big[\epsilon_e(t) - Z(t,v)\big], \quad Z(0,v) = 0, \tag{7}$$

where $\Gamma(v)$ is given by (A.5). The stress $\sigma$ reads

$$\sigma(t) = E\big(1-\phi(t)\big)\left[\epsilon_e(t) - \int_0^\infty f(v)Z(t,v)\,dv\right], \tag{8}$$

where $E$ stands for Young's modulus.

Stress–strain relations (2)–(8) involve nine adjustable parameters: $E, a_1, a_2, R_1, R_2, S_1, S_2, \gamma, \Sigma$.

The constants $\gamma$ and $\Sigma$ are found by fitting observations in short-term relaxation tests. Approximation of the relaxation curves reported in Drozdov et al. (2009) implies that these quantities are independent of $\chi$ and read $\gamma = 0.11$ s$^{-1}$, $\Sigma = 13.1$. Treatment of $\gamma$ and $\Sigma$ as constants means that the effect of cyclic viscoplasticity on the viscoelastic response is disregarded.

The elastic modulus $E$ is determined by matching stress–strain diagrams under stretching of virgin specimens. Approximation of the loading curves with cross-head speed $\dot{d} = 100$ mm/min reported in Drozdov et al. (2009) implies that $E = 2.26$ GPa at $\chi = 0$ wt.% and $E = 2.85$ GPa at $\chi = 2$ wt.%. The assumption that $E$ is constant distinguishes the present approach from conventional concepts in damage mechanics that postulate a decay in elastic modulus under deformation.

### 3.2 Evolution equations

To reduce the number of adjustable parameters, it is postulated that $R_1$ is independent of $n$ and reads $R_1 = 1$.

To describe evolution of the remaining parameters, $a_1$, $a_2$, $R_2$, $S_1$, $S_2$, with number of cycles, we introduce plastic work

$$W_{\rm p}(t) = \int_0^t \sigma(s) \frac{{\rm d}\epsilon_{\rm p}}{{\rm d}t}(s) {\rm d}s$$

as the measure of changes in internal structure of nanocomposites driven by damage accumulation. The following scenario is proposed:

1. Coefficients $a_1$ and $a_2$ decrease monotonically with number of cycles and vanish when $n$ becomes relatively large. The decay in these parameters is described by the equations

$$a_1 = a_{10} - a_{11} W_{\rm p}^{\rm min}, \qquad a_2 = a_{20} - a_{21} W_{\rm p}^{\rm max}, \tag{9}$$

   where $a_{10}$, $a_{11}$, $a_{20}$, $a_{21}$ are constants, and $W_{\rm p}^{\rm min}$, $W_{\rm p}^{\rm max}$ are plastic works at instants when strain $\epsilon$ reaches its minimum and maximum values, respectively.
2. Coefficient $R_2$ decreases monotonically with number of cycles and vanishes at relatively large values of $n$. Depending on the loading program, the decay in $R_2$ is described either by the logarithmic equation

$$\log R_2 = R_{20} - R_{21} W_{\rm p}^{\rm max}, \tag{10}$$

   or by the linear equation

$$R_2 = R_{20} - R_{21} W_{\rm p}^{\rm max}, \tag{11}$$

   where $R_{20}$, $R_{21}$ are constants.
3. During an initial transition period (when $a_1$ and $a_2$ decay to zero), coefficients $S_1$ and $S_2$ strongly decrease with number of cycles. Afterwards, these quantities evolve linearly with plastic work

$$S_1 = S_{10} + S_{11} W_{\rm p}^{\rm min}, \qquad S_2 = S_{20} + S_{21} W_{\rm p}^{\rm max}, \tag{12}$$

   where $S_{10}$, $S_{11}$, $S_{20}$, $S_{21}$ are constants.

After an initial transition period (along which parameters $a_1$, $a_2$, and $R_2$ vanish), mechanical response of a polymer/clay nanohybrid under cyclic deformation is determined by five adjustable parameters: (i) $E$ stands for elastic modulus, (ii) $\gamma$ determines relaxation rate, (iii) $\Sigma$ characterizes distribution of relaxation times, (iv) $S_1$ and $S_2$ denote rates of plastic flow in the amorphous matrix under loading and unloading.

## 4 Fitting of observations

Adjustable parameters in the constitutive equations are found by fitting the experimental data depicted in Figs. 5 and 6. Each set of observations is matched separately.

### 4.1 Loading

The response of a polymer nanocomposite under stretching is determined by two parameters, $a_1$ and $S_1$. These quantities are found by fitting observations with the help of the following algorithm. To approximate the first loading path, we fix some intervals $[0, a^\circ]$ and $[0, S^\circ]$, where $a_1$ and $S_1$ are located, and divide these intervals into $J = 10$ sub-intervals by the points $a^{(i)} = i\Delta a$, $S^{(j)} = j\Delta S$ with $\Delta a = a^\circ/J$, $\Delta S = S^\circ/J$ $(i, j = 0, 1, \ldots, J-1)$. For each pair $\{a^{(i)}, S^{(j)}\}$, stress–strain relations (2)–(8) are integrated numerically from $\epsilon = 0$ to $\epsilon = \epsilon^{\max}$, where $\epsilon^{\max}$ stands for maximum strain under stretching. Integration over time is performed by the Runge–Kutta method with step $\Delta t = 0.01$ s. Integrals in (6) and (8) are evaluated by the Simpson method with step $\Delta v = 2$ and $M = 20$ steps. Parameters $a_1$ and $S_1$ are calculated from the condition of minimum of the function $F = \sum_k [\sigma^{\exp}(\epsilon_k) - \sigma^{\text{num}}(\epsilon_k)]^2$, where summation is performed over all strains $\epsilon_k$ at which the observations are presented, $\sigma^{\exp}$ is the stress measured in the test, and $\sigma^{\text{num}}$ is given by (8). Afterwards, the initial intervals are replaced with new intervals $[a_1 - \Delta a, a_1 + \Delta a]$, $[S_1 - \Delta S, S_1 + \Delta S]$, and the calculations are repeated.

Subsequent loading paths are approximated by means of the same algorithm. The only difference is that the right boundary of the interval $[0, a^\circ]$ at the $n$th cycle is chosen from the condition $a^\circ \le a_1(n-1)$, where $a_1(n-1)$ is the best-fit value of $a_1$ at the $(n-1)$th cycle. When $a_1$ vanishes at $n'$th cycle, fitting of observations at the $n$th cycle with $n > n'$ is performed with the only adjustable parameter $S_1$.

### 4.2 Unloading

The response of a polymer nanocomposite under retraction is determined by three parameters, $a_2$, $R_2$, and $S_2$. These quantities are found by means of the above algorithm where the right boundaries of all intervals $[0, a^\circ]$, $[0, R^\circ]$, and $[0, S^\circ]$ are chosen from the conditions $a^\circ \le a_2(n-1)$, $R^\circ \le R_2(n-1)$, and $S^\circ \le S_2(n-1)$, which guarantee monotonic decay of these coefficients with number of cycles. After the initial transition period, when $a_2$ and $R_2$ vanish, this restriction on $S_2$ is removed.

### 4.3 Discussion

When $a_1$, $a_2$, $R_2$, $S_1$, $S_2$ are determined for each cycle of loading–retraction, plastic work $W_p$ is calculated by integration of the stress–strain relations, and the adjustable parameters are plotted versus $W_p$ in Figs. 9–13.

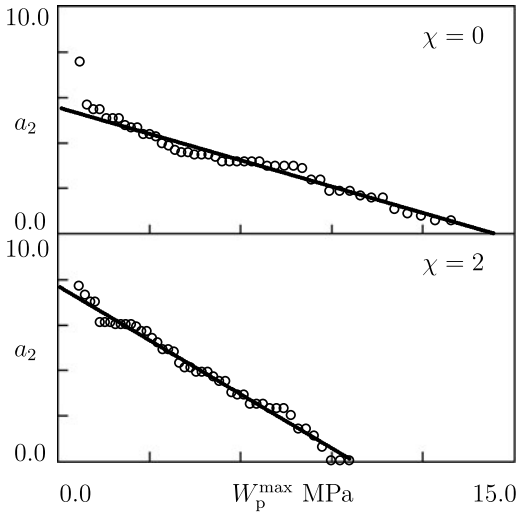


**Fig. 10** Parameter $a_2$ versus plastic work $W_p^{max}$. *Circles*: treatment of observations in cyclic tests on nanocomposites with various clay contents $\chi$ wt.%. *Solid lines*: approximation of the data by (9)

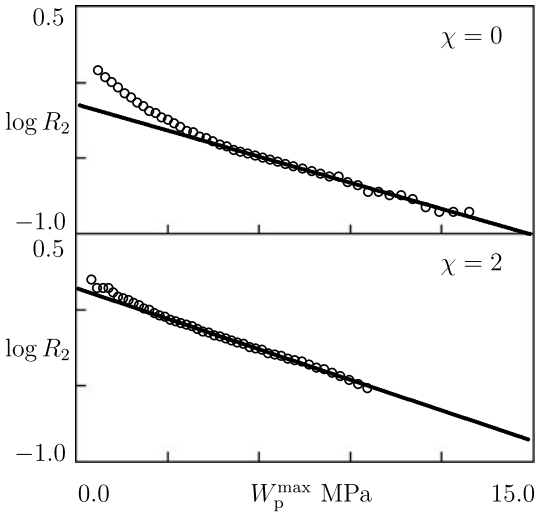


**Fig. 11** Parameter $R_2$ versus plastic work $W_p^{max}$. *Circles*: treatment of observations in cyclic tests on nanocomposites with various clay contents $\chi$ wt.%. *Solid lines*: approximation of the data by (10)

The experimental dependencies $a_1(W_p^{min})$ and $a_2(W_p^{max})$ are reported in Figs. 9 and 10 together with their approximations by (9) where coefficients are calculated by the least-squares technique. These figures demonstrate that $a_1$ and $a_2$ decrease linearly with plastic work and vanish when fatigue failure of specimens occurs. The best-fit values of $a_1$ and $a_2$ at the first and last cycles are weakly affected by nanoclay content $\chi$. However, slopes $a_{11}$ and $a_{21}$ for nanocomposite with $\chi = 2$ wt.% of filler exceed those for neat polypropylene practically by twice (due to more pronounced growth of $W_p$ at $\chi = 0$ wt.%).

The experimental diagrams $R_2(W_p^{max})$ are presented in Fig. 11 where the data are approximated by (10). This figure shows that the decay in $R_2$ with plastic work is weakly affected by clay content ($R_{21}$ at $\chi = 2$ wt.% exceeds that at $\chi = 0$ wt.% by 17%).

Evolution of coefficients $S_1$ and $S_2$ with plastic work $W_p$ is illustrated in Figs. 12 and 13. According to these figures, $S_1$ and $S_2$ decrease monotonically and become independent of $W_p$ at the end of the initial transition period. The ultimate value of $S_1$ is weakly affected by

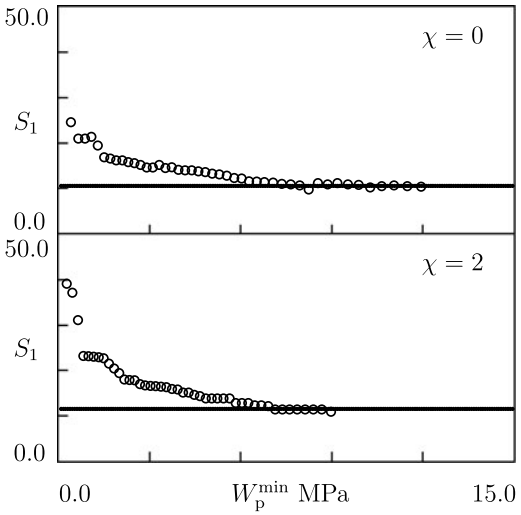


**Fig. 12** Parameter $S_1$ versus plastic work $W_p^{min}$. *Circles*: treatment of observations in cyclic tests on nanocomposites with various clay contents $\chi$ wt.%. *Solid lines*: approximation of the data by (12)

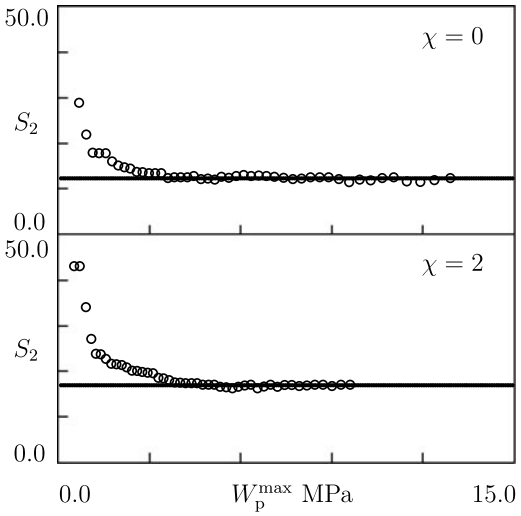


**Fig. 13** Parameter $S_2$ versus plastic work $W_p^{max}$. *Circles*: treatment of observations in cyclic tests on nanocomposites with various clay contents $\chi$ wt.%. *Solid lines*: approximation of the data by (12)

clay content ($S_{10}$ at $\chi = 2$ wt.% exceeds $S_{10}$ at $\chi = 0$ wt.% by 7%), whereas the ultimate value of $S_2$ at $\chi = 2$ wt.% exceeds that for neat polypropylene by 35%.

Comparison of coefficients in the stress–strain relations leads to the conclusion that a strong increase in fatigue resistance due to reinforcement of polypropylene with nanoclay may be associated with growth of rates of plastic flow in the amorphous matrix under loading $S_1$ and retraction $S_2$.

### 4.4 Numerical simulation

Although the above analysis seems reasonable, a number of questions arises:

1. Adjustable parameters in the constitutive equations were found to ensure the best fit of the experimental stress–strain diagrams. How accurate approximation of observations can be reached within the proposed model?

2. To characterize evolution of coefficients $a_1$, $a_2$, $R_2$, $S_1$, and $S_2$ with number of cycles, plastic work $W_p$ was chosen as an internal variable. Why this quantity is more suitable for modeling than others (for example, plastic strain $\epsilon_p$ or plastic strains $\epsilon_{p1}$ and $\epsilon_{p2}$ in crystalline and amorphous phases)?
3. Fatigue failure of specimens occurs when coefficients $a_1$ and $a_2$ vanish. Is this a coincidence? What is a physical mechanism of breakage of specimens under ratcheting?

To provide some answers to these questions, numerical simulation is conducted of the stress–strain relations with the adjustable parameters depicted in Figs. 9–13. To examine the quality of the approximations (9)–(12), integration of the constitutive equations for the first 25 cycles is performed with the best-fit parameters $a_1$, $a_2$, $R_2$, $S_1$, $S_2$, while integration for subsequent cycles of loading–retraction is carried out by using (9), (10), and (12). Results of calculations are depicted in Figs. 5 and 6. These figures demonstrate excellent agreement between the experimental stress–strain diagrams and predictions of the model for the first 40 cycles (stages of primary and secondary fatigue) and quite an acceptable prediction of observations at the stage of tertiary fatigue (slight deviations between experimental data and results of simulation are visible along the last two cycles before breakage only).

To examine validity of the model, we compare experimental dependencies $\epsilon^{\max}(n)$ and $\epsilon^{\min}(n)$ with results of numerical analysis for 50 cycles of loading–retraction in Figs. 7 and 8. These figures reveal good agreement between the observations and the results of numerical analysis up to breakage of specimens under ratcheting.

To understand why failure of specimens is observed under stress-controlled loading, maximum $\epsilon_p^{\max}$ and minimum $\epsilon_p^{\min}$ plastic strains per cycle are calculated and plotted versus $n$ in Figs. 14 and 15. These figures demonstrate that transition to tertiary fatigue is accompanied by a pronounced (exponential) growth of plastic strains. In order to associate this growth with deformations in specific phases, maximum and minimum plastic strains in the crystalline $\epsilon_{p1}^{\max}$, $\epsilon_{p1}^{\min}$ and amorphous $\epsilon_{p2}^{\max}$, $\epsilon_{p2}^{\min}$ regions are also reported. Figures 14 and 15 show that fatigue failure is driven by a pronounced growth of plastic strain in the crystalline phase. Although plastic strains $\epsilon_{p1}^{\max}$ at the 50th cycle calculated at $\chi = 0$ and $\chi = 2$ wt.% differ from each other, this does not indicate that the mechanisms of failure are different: the increase in $\epsilon_{p1}^{\max}(n)$ is so strong that its value exceeds 0.2 within 55 cycles of oscillations for

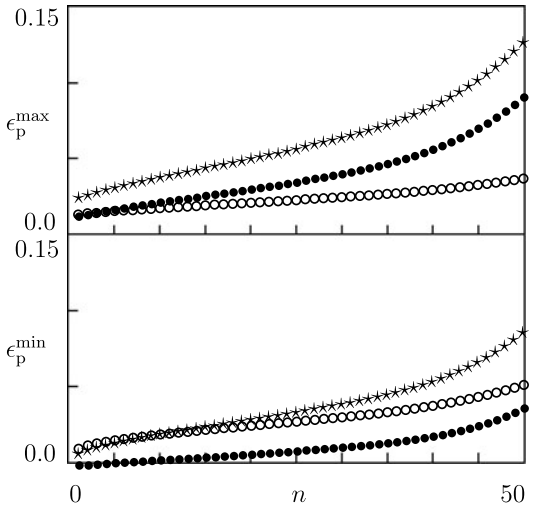


**Fig. 14** Maximum $\epsilon_p^{\max}$ and minimum $\epsilon_p^{\min}$ plastic strains versus number of cycles $n$. *Symbols*: predictions of the model for the cyclic test with $\sigma^{\max} = 32$ MPa and $\sigma^{\min} = 1$ MPa on nanocomposite with $\chi = 0$ wt.% of clay ($\star$ total plastic strain $\epsilon_p$; $\bullet$ plastic strain in the crystalline phase $\epsilon_{p1}$; $\circ$ plastic strain in the amorphous phase $\epsilon_{p2}$)

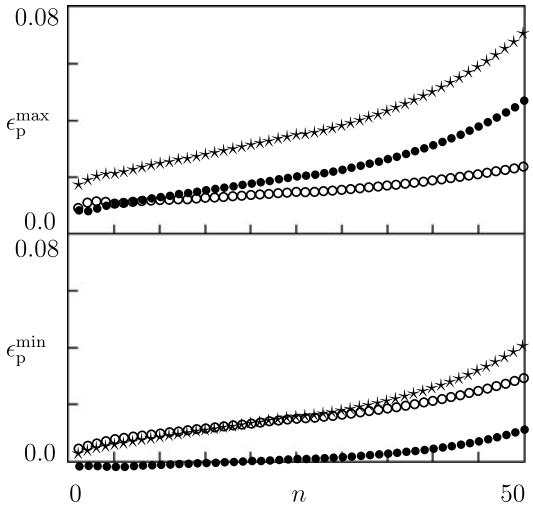


**Fig. 15** Maximum $\epsilon_p^{max}$ and minimum $\epsilon_p^{min}$ plastic strains versus number of cycles $n$. *Symbols*: predictions of the model for the cyclic test with $\sigma^{max} = 35$ MPa and $\sigma^{min} = 1$ MPa on nanocomposite with $\chi = 2$ wt.% of clay ($\star$ total plastic strain $\epsilon_p$; $\circ$ plastic strain in the amorphous phase $\epsilon_{p1}$; $\bullet$ plastic strain in the crystalline phase $\epsilon_{p2}$)

both concentrations of filler (appropriate data are not presented as the model is directed to describe the mechanical response at small strain only).

## 5 Mixed deformation program

To demonstrate ability of the constitutive model to describe the viscoelastic and viscoplastic responses under cyclic deformation with other loading programs, the mechanical behavior of polypropylene is analyzed in uniaxial tensile tests with a mixed program, when a specimen is stretched up to some maximum strain $\epsilon^{max}$ and unloaded down to a fixed minimum stress $\sigma^{min}$.

A series of uniaxial cyclic tests is performed at room temperature with maximum strains $\epsilon^{max} = 0.08$, 0.12, and 0.16, minimum stress $\sigma^{min} = 1$ MPa, and cross-head speed $\dot{d} = 100$ mm/min. Each test involved 150 cycles of loading–retraction.

A typical stress–strain diagram (corresponding to $\epsilon^{max} = 0.12$) is reported in Fig. 16. This figure shows that in cyclic tests with mixed program:

1. Loading and unloading paths are strongly nonlinear.
2. Hysteresis energy decreases noticeably with number of cycles.
3. The stress–strain diagram rotates counter-clockwise with growth of $n$.

Evolution of maximum stress per cycle $\sigma^{max}$ and minimum strain per cycle $\epsilon^{min}$ with $n$ is illustrated in Fig. 17 which shows that $\sigma^{max}$ substantially decreases within the first 20 cycles and becomes practically constant afterwards, whereas $\epsilon^{min}$ increases monotonically with number of cycles.

Adjustable parameters in the constitutive equations are determined by matching the stress–strain curve for the first 50 cycles of oscillations. These quantities are presented in Figs. 18 and 19, where the data are approximated by (9), (11), and (12). The fitting procedure coincides with that used in the analysis of cyclic tests with stress-controlled program.

Figure 18 demonstrates that $a_1$ and $a_2$ decrease linearly with corresponding plastic work ($W_p^{min}$ or $W_p^{max}$), and vanish after an initial transition period (about 10 cycles). Coefficient $R_2$ decreases with $W_p^{max}$ and vanishes together with $a_1$ and $a_2$. This distinguishes mechanical responses of polypropylene under stress-controlled and mixed programs: in the former

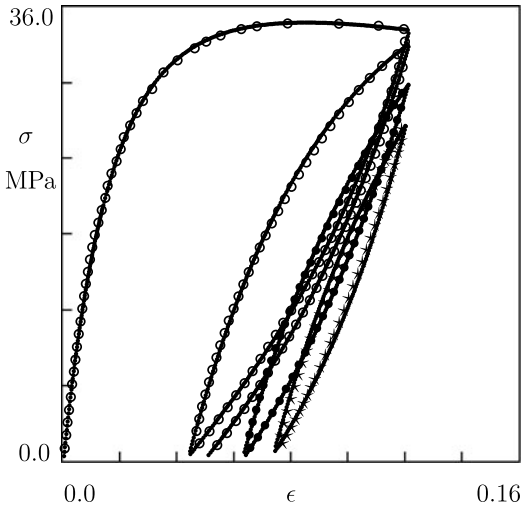


**Fig. 16** Stress $\sigma$ versus strain $\epsilon$. *Symbols*: observations on polypropylene in the cyclic test with $\epsilon^{\max} = 0.12$ and $\sigma^{\min} = 1$ MPa: $\circ$ $n = 1, 2$; $\bullet$ $n = 10$; $\star$ $n = 50$. *Solid lines*: results of numerical simulation.

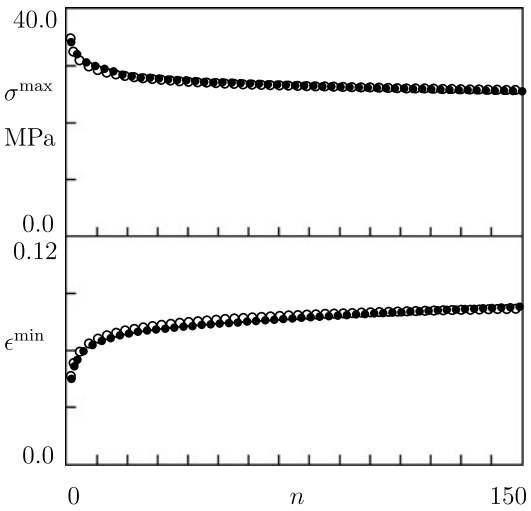


**Fig. 17** Maximum stress $\sigma^{\max}$ and minimum strain $\epsilon^{\min}$ versus number of cycles $n$. *Unfilled circles*: observations on polypropylene in the cyclic test with $\epsilon^{\max} = 0.12$ and $\sigma^{\min} = 1$ MPa. *Filled circles*: predictions of the model

case, $R_2$ remained positive up to breakage of specimens. It appears that the difference between (10) and (11) is not dramatic: an accurate approximation of the data depicted in Fig. 18 shows that (10) adequately fits the experimental dependence for the first three–four cycles, whereas (11) is more suitable for subsequent cycles of loading–retraction.

According to Fig. 19, parameter $S_1$ increases weakly, but monotonically with plastic work. After the transition period, its dependence on $W_{\mathrm{p}}^{\min}$ is correctly approximated by (12). Coefficient $S_2$ decreases with $W_{\mathrm{p}}^{\max}$ within the transition period and grows with plastic work afterwards.

To validate (12), numerical simulation is conducted of the stress–strain relations for 150 cycles of loading–retraction. For the first 50 cycles of oscillations, integration of the constitutive equations is performed with the adjustable parameters depicted in Figs. 18 and 19, whereas for the other 100 cycles, (12) is used. Results of numerical analysis are reported in

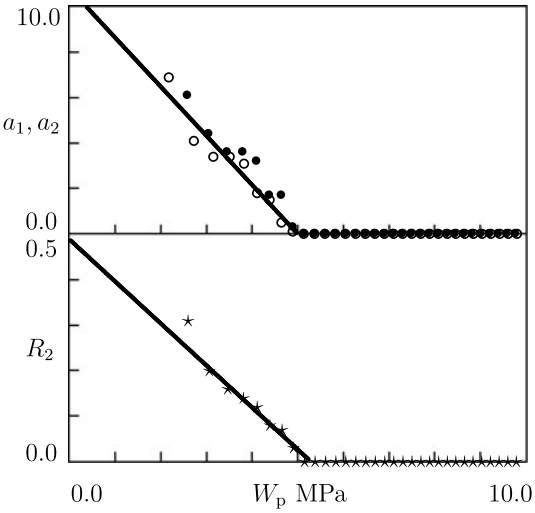


**Fig. 18** Parameters $a_1$ (∘), $a_2$ (•), and $R_2$ (⋆) versus plastic work $W_p$. *Symbols*: treatment of observations on polypropylene in the cyclic test with $\epsilon^{max} = 0.12$ and $\sigma^{min} = 1$ MPa. *Solid lines*: approximation of the data by (9) and (11)

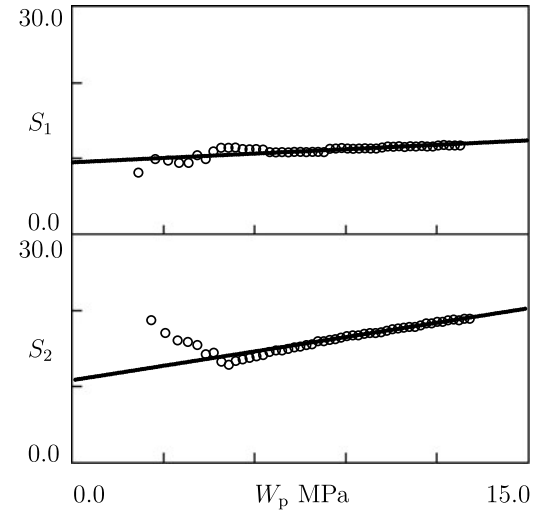


**Fig. 19** Parameters $S_1$ and $S_2$ versus plastic work $W_p$. *Circles*: treatment of observations on polypropylene in the cyclic test with $\epsilon^{max} = 0.12$ and $\sigma^{min} = 1$ MPa. *Solid lines*: approximation of the data by (12)

Fig. 17 which reveals good agreement between predictions of the model and the experimental data.

To examine a difference between the viscoelastoplastic responses of polypropylene in stress-controlled cyclic tests (where fatigue failure occurs) and cyclic tests with a mixed program (where no breakage of samples is observed), evolution of maximum and minimum plastic strains with number of cycles is studied numerically. Results of numerical simulation are depicted in Fig. 20. This figure shows that maximum plastic strains $\epsilon_p^{max}$, $\epsilon_{p1}^{max}$, and $\epsilon_{p2}^{max}$ remain practically independent of $n$. After the initial transition period, minimum plastic strain in the amorphous matrix $\epsilon_{p2}^{min}$ is weakly affected by number of cycles, whereas minimum plastic strain in the crystalline phase $\epsilon_{p1}^{min}$ and total minimum plastic strain $\epsilon_p^{min}$ grow monotonically with $n$.

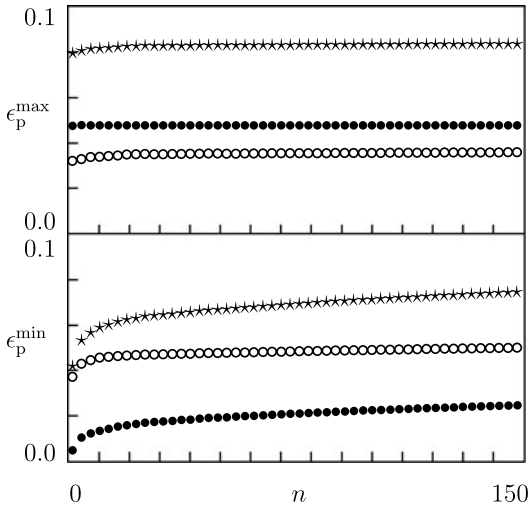


**Fig. 20** Maximum $\epsilon_p^{max}$ and minimum $\epsilon_p^{min}$ plastic strains versus number of cycles $n$. *Symbols*: predictions of the model for the cyclic test on polypropylene with $\epsilon^{max} = 0.12$ and $\sigma^{min} = 1$ MPa ($\star$ total plastic strain $\epsilon_p$; $\bullet$ plastic strain in the crystalline phase $\epsilon_{p1}$; $\circ$ plastic strain in the amorphous phase $\epsilon_{p2}$)

The data depicted in Figs. 19 and 20 unambiguously demonstrate that plastic strains $\epsilon_p$, $\epsilon_{p1}$, and $\epsilon_{p2}$ cannot be used as internal variables: Fig. 19 show that $S_2$ strongly increases with number of cycles, while maximum plastic strains remain independent of $n$.

To check whether $W_p$ is a proper candidate for internal variable, stress–strain diagrams in cyclic tests with mixed loading program and various $\epsilon^{max}$ are approximated until coefficients $a_1$, $a_2$ and $R_2$ vanish. To compare rates of their decay with $W_p$, auxiliary variables are introduced

$$\bar{a}_1 = \frac{a_1}{a_2(1)}, \quad \bar{a}_2 = \frac{a_2}{a_2(1)}, \quad \bar{R}_2 = \frac{R_2}{R_2(1)},$$

where $a_2(1)$ and $R_2(1)$ stand for coefficients $a_2$ and $R_2$ at first retraction (these parameters read 3.0 and 0.65 at $\epsilon^{max} = 0.08$, 6.1 and 0.31 at $\epsilon^{max} = 0.12$, 8.0 and 0.22 at $\epsilon^{max} = 0.16$). The data are depicted in Fig. 21 where the experimental dependencies $\bar{a}_1(W_p^{min})$, $\bar{a}_2(W_p^{max})$, and $\bar{R}_2(W_p^{max})$ are approximated by the equations, similar to (9) and (11),

$$\bar{a}_1 = a_{10} - a_{11} W_p^{min}, \qquad \bar{a}_2 = a_{20} - a_{21} W_p^{max}, \qquad \bar{R}_2 = R_{20} - R_{21} W_p^{max} \tag{13}$$

with coefficients calculated by the least-squares method. Although scatter of the data is noticeable, coincidence of the slopes of corresponding curves in Fig. 21 confirms that $W_p$ may be treated as an internal variable that accounts for damage accumulation under cyclic deformations with mixed program.

## 6 Strain-controlled deformation program

Our aim now is to demonstrate ability of the constitutive model to predict observations under cyclic deformation with a strain-controlled program (oscillations between fixed maximum strain $\epsilon^{max}$ and minimum strain $\epsilon^{min}$). For this purpose, uniaxial tensile cyclic test (100 cycles) was performed on polypropylene with cross-head speed $\dot{d} = 100$ mm/min, maximum strain $\epsilon^{max} = 0.07$, and minimum strain $\epsilon^{min} = 0.04$. The test was conducted on the same grade of polypropylene as cyclic tests with stress-controlled and mixed programs. The only difference is that dumbbell specimens were injection-molded under different conditions (a

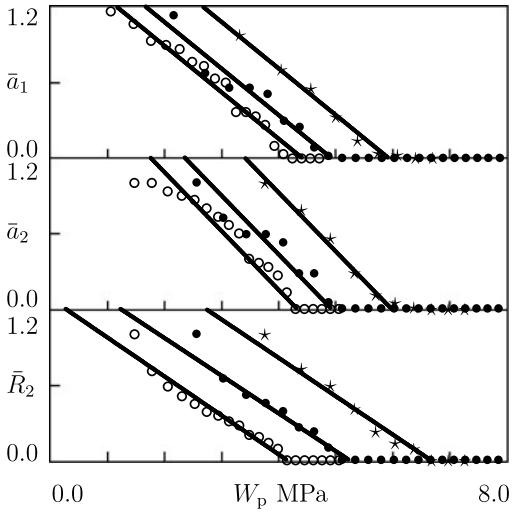


**Fig. 21** Parameters $\bar{a}_1$, $\bar{a}_2$, and $\bar{R}_2$ versus plastic work $W_p$. *Symbols*: treatment of observations on polypropylene in cyclic tests with $\epsilon^{max} = 0.08$ ($\circ$), $\epsilon^{max} = 0.12$ ($\bullet$), $\epsilon^{max} = 0.16$ ($\star$). *Solid lines*: approximation of the data by (13)

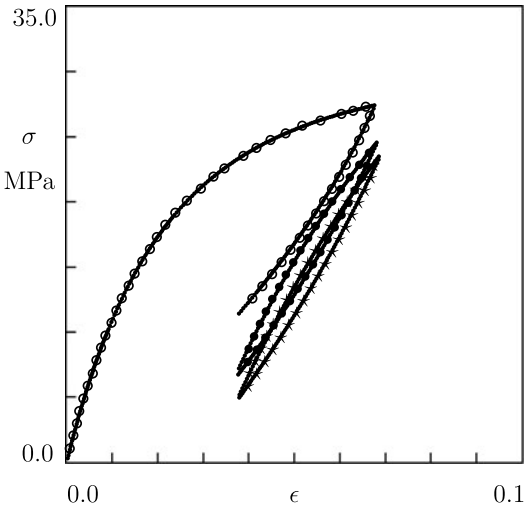


**Fig. 22** Stress $\sigma$ versus strain $\epsilon$. *Symbols*: observations on polypropylene in the cyclic test with $\epsilon^{max} = 0.07$ and $\epsilon^{min} = 0.04$: $\circ$ $n = 1$; $\bullet$ $n = 10$; $\star$ $n = 30$. *Solid lines*: results of numerical simulation

lower temperature of the mold) which led to lower degree of crystallinity and lower Young's modulus ($E = 1.42$ GPa).

The experimental stress–strain diagram is reported in Fig. 22. To avoid overlapping of observations, only data for the first, 10th, and 30th cycle are depicted. The following conclusions are drawn:

1. Loading and unloading paths of the stress–strain diagram are strongly nonlinear.
2. Hysteresis energy decreases noticeably with number of cycles.
3. Stress–strain curves rotate counter-clockwise with growth of $n$.
4. The secant elastic modulus $E_s$ (defined as slope of the straight line connecting points when strain rate changes its sign) increases monotonically with $n$ (cyclic strengthening).

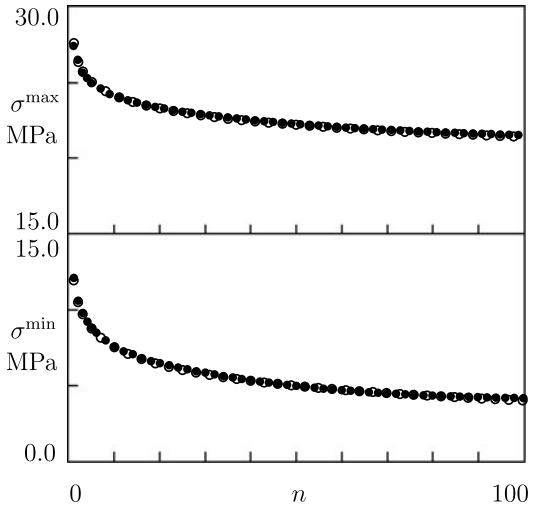


**Fig. 23** Maximum $\sigma^{\max}$ and minimum $\sigma^{\min}$ stresses versus number of cycles $n$. *Unfilled circles*: observations on polypropylene in the cyclic test with $\epsilon^{\max} = 0.07$ and $\epsilon^{\min} = 0.04$. *Filled circles*: predictions of the model

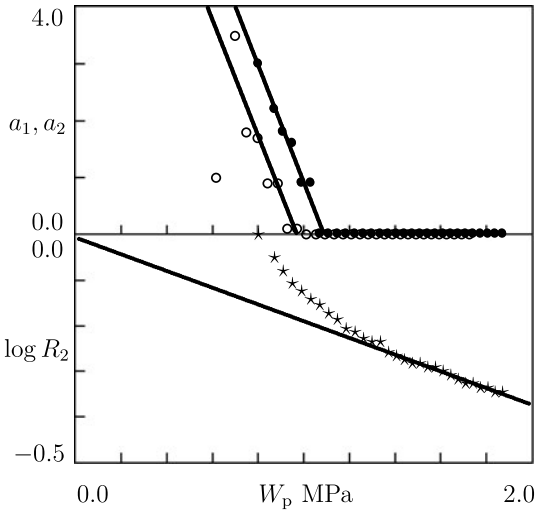


**Fig. 24** Parameters $a_1$ (∘), $a_2$ (•), and $R_2$ (⋆) versus plastic work $W_p$. *Symbols*: treatment of observations on polypropylene in the cyclic test with $\epsilon^{\max} = 0.07$ and $\epsilon^{\min} = 0.04$. *Solid lines*: approximation of the data by (9) and (10)

Maximum $\sigma^{\max}$ and minimum $\sigma^{\min}$ stresses are plotted versus number of cycles in Fig. 23. This figure shows that both stresses decrease strongly with $n$, but the decay in $\sigma^{\min}$ occurs more pronouncedly.

To find adjustable parameters in the constitutive equations, experimental stress–strain diagrams are approximated for the first 30 cycles of oscillations. Coefficients $a_1$, $a_2$, and $R_2$ are plotted versus plastic work $W_p$ in Fig. 24 where the data are approximated by (9) and (10). This figure shows that (9) and (10) correctly fit the observations.

Comparison of Figs. 18 and 24 demonstrates the same kinetics of evolution of coefficients $a_1$ and $a_2$ (these quantities decay to zero practically linearly with $W_p$), but different kinetics of decrease in $R_2$. Under cyclic deformation with mixed program, the latter quantity vanishes simultaneously with $a_1$ and $a_2$ and decreases linearly with $W_p$, whereas under cyclic deformation with strain-controlled program, $R_2$ weakly decays with $W_p$ following the same pattern (10) as under stress-controlled cyclic loading.

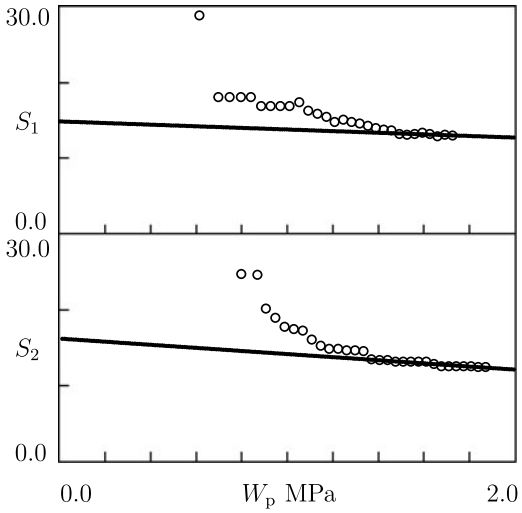


**Fig. 25** Parameters $S_1$ and $S_2$ versus plastic work $W_p$. *Circles*: treatment of observations on polypropylene in the cyclic test with $\epsilon^{max} = 0.07$ and $\epsilon^{min} = 0.04$. *Solid lines*: approximation of the data by (12)

Parameters $S_1$ and $S_2$ are plotted versus plastic work $W_p$ in Fig. 25. The data after the initial transition period (within which $a_1$ and $a_2$ vanish) are matched by (12) with coefficients determined by the least-squares method. Figure 25 confirms accuracy of approximation of the data by (12).

Comparison of Figs. 12, 13, 19, and 25 reveals different kinetics of evolution of rates of plastic flow in the amorphous phase under cyclic loading: $S_1$ and $S_2$ (i) remain constant under stress-controlled program, (ii) increase under mixed program, and (iii) decrease under strain-controlled program. This observation can be taken into account with the help of the following generalization of (12):

$$\begin{aligned} S_1 &= S_{10} - S_{11} W_p^{min} H\left(\frac{d(\sigma^{max} - \sigma^{min})}{dW_p^{min}}\right), \\ S_2 &= S_{20} - S_{21} W_p^{max} H\left(\frac{d(\sigma^{max} - \sigma^{min})}{dW_p^{max}}\right), \end{aligned} \tag{14}$$

where $H$ stands for the Heaviside function:

$$H(x) = 1 \quad (x > 0), \qquad H(0) = 0, \qquad H(x) = -1 \quad (x < 0).$$

To confirm validity of approximations (9), (10), and (12), numerical simulation is conducted of the stress–strain relations for 100 cycles of loading–retraction. For the first 30 cycles, integration of the governing equations is performed with parameters $a_1$, $a_2$, $R_2$, $S_1$, $S_2$ depicted in Figs. 24 and 25, whereas for subsequent cycles, (9), (10), and (12) are employed. Results of numerical analysis are depicted in Fig. 23. This figure reveals good agreement between the experimental data for maximum and minimum stresses and predictions of the model.

To characterize plastic flow in polypropylene under strain-controlled deformation program, maximum and minimum plastic strains are plotted versus number of cycles in Fig. 26. This figure demonstrates that plastic deformation in the crystalline phase remains constant and shows slow growth of total plastic strains $\epsilon_p^{max}$ and $\epsilon_p^{min}$ driven by a weak increase in plastic strains in the amorphous matrix.

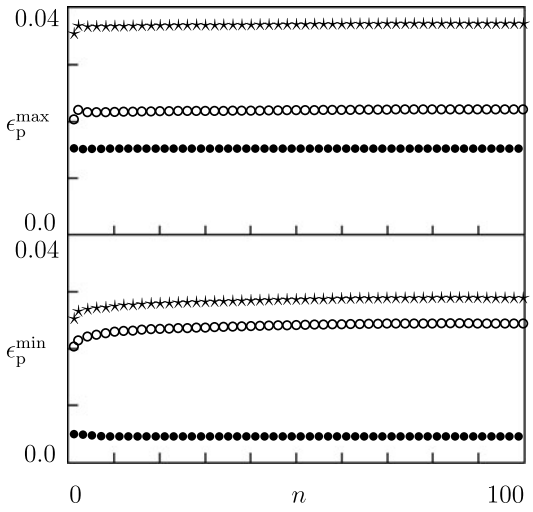


**Fig. 26** Maximum $\epsilon_p^{max}$ and minimum $\epsilon_p^{min}$ plastic strains versus number of cycles $n$. *Symbols*: predictions of the model for the cyclic test on polypropylene with $\epsilon^{max} = 0.07$ and $\epsilon^{min} = 0.04$ ($\star$ total plastic strain $\epsilon_p$; $\bullet$ plastic strain in the crystalline phase $\epsilon_{p1}$; $\circ$ plastic strain in the amorphous phase $\epsilon_{p2}$)

## 7 Concluding remarks

Observations have been reported on polypropylene/nanoclay hybrids with various concentrations of filler in tensile cyclic tests with stress-controlled program. Experimental data show that reinforcement of polypropylene with nanoclay resulted in strong (by several times) reduction in ratcheting strain and substantial (by two orders of magnitude) growth of number of cycles to failure. The most pronounced improvement of fatigue resistance is reached when concentration of nanoclay equals 2 wt.%.

A constitutive model is developed in cyclic viscoelasticity and viscoplasticity of polymer nanocomposites by using a two-step approach. First, stress–strain relations are derived for an individual cycle of loading–retraction by using the Clausius–Duhem inequality. Afterwards, some coefficients in the governing equations are presumed to slowly change with number of cycles, and kinetic equations are proposed for evolution of these quantities driven by damage accumulation. Specific plastic work is selected as an internal variable in evolution equations for rates of viscoplastic flow, and this choice is confirmed by comparison of observations in cyclic tests with mixed deformation program and various maximum strains.

The stress–strain equations involve eight material parameters. Three of them are determined in independent tests (tension with a constant strain rate and short-term relaxation tests). The other five quantities are split into two groups: three parameters strongly decrease and vanish within an initial transition period (a couple of dozens of cycles); the last two parameters slowly evolve with the number of cycles following (14).

Ability of the model to describe experimental data is examined by analyzing observations in tensile tests with stress-controlled (oscillations between fixed minimum and maximum stresses), mixed (oscillations between a maximum strain and a minimum stress), and strain-controlled (oscillations between fixed minimum and maximum strains) programs. Coefficients in the constitutive equations are found by fitting stress–strain diagrams along the first several cycles (30 to 50, depending on the deformation program). Afterwards, predictions of the model are compared with observations in tests where number of cycles strongly exceeds that used for determination of material constants. Good agreement is revealed between results of numerical simulation and experimental data.

Comparison of the viscoelastic and viscoplastic responses of polymer specimens subjected to different deformation programs reveals the presence of two independent mecha-

nisms of damage accumulation responsible for different kinetics of evolution of coefficients $a_1$ and $a_2$, on the one hand, and $R_2$, on the other. The linear decay in $a_1$ and $a_2$ with plastic work $W_p$ observed under all deformation programs may be attributed to lamellar fragmentation in spherulites. The monotonic reduction in $R_2$ whose kinetics coincides with that for $a_1$ and $a_2$ under mixed deformation program and differs noticeably from the kinetics of decrease in $a_1$ and $a_2$ under stress- and strain-controlled loading programs may be associated with growth of micro-voids in the amorphous matrix. Experimental data reported in this study are, however, insufficient for an unambiguous explanation of this phenomenon and further analysis is required.

Numerical simulation demonstrates that fatigue failure of specimens under stress-controlled loading is induced by a pronounced growth of plastic deformation in the crystalline phase. In cyclic tests with mixed and strain-controlled programs (where breakage of specimens does not occur) maximum and minimum plastic strains in crystallites remain practically independent of number of cycles.

Comparison of material parameters for neat and clay-reinforced polypropylene leads to the conclusion that enhancement of fatigue resistance may be ascribed to acceleration of plastic flow in the matrix driven by sliding of clay platelets in their stacks, as well as sliding of polymer chains along the surfaces of clay particles.

**Acknowledgements** Financial support by the European Commission (project Nanotough–213436) and Danish Agency for Science, Technology and Innovation (project RK 2010–2012 B4) is gratefully acknowledged.

## Appendix: Constitutive model

This section focuses on derivation of constitutive equations in viscoelastiplasticity of polymer nanocomposites for an individual cycle of loading–retraction. Our purpose is to develop stress–strain relations with a relatively small number of adjustable parameters to be applied for description of the mechanical response under multi-cycle loading with an arbitrary three-dimensional deformation at small strains.

To construct a model with a reasonable number of material constants, a homogenization concept is employed. A nanocomposite with a complicated microstructure (a semicrystalline matrix reinforced with randomly distributed clay platelets and their stacks) is replaced with an equivalent isotropic medium, whose mechanical response resembles that of the hybrid. An incompressible, inhomogeneous, transient, non-affine network of chains bridged by junctions is chosen as the equivalent continuum (Drozdov and Christiansen 2007).

The incompressibility assumption means that deformation of nanocomposite is volume-preserving. This hypothesis is confirmed by our observations in uniaxial tensile tests with various cross-head speeds where longitudinal and transverse strains were measured simultaneously (Drozdov et al. 2011).

The concept of transient networks was suggested for the analysis of time-dependent behavior of polymers by Tanaka and Edwards (1992). This theory associates relaxation of stresses with rearrangement of chains in a polymer network: detachment of active chains from their junctions and attachment of dangling chains to the network.

The assumption about heterogeneity of the network means that the polymer network is thought of as an ensemble of meso-regions where rearrangement of chains occurs with different rates. This statement is tantamount to the conventional assertion about the existence of a spectrum of relaxation times.

Non-affinity of the network means that junctions between chains slip with respect to their reference positions under deformation. Slippage of junctions reflects plastic flow in polymer nanocomposite. To account for different kinetics of plastic deformation in amorphous and crystalline domains, the entire plastic strain is split into the sum of two components whose evolution is governed by different flow rules.

A shortcoming of the present model is that it disregards interactions between different phases, in particular the presence of interfaces between the matrix and clusters of clay platelets (Sheng et al. 2004; Qiao and Brinson 2009; Kaushik et al. 2011; Li et al. 2011a, 2011b), as well as the presence of inter-phases between amorphous matrix and spherulites and near the fold and stem surfaces (Rastogi et al. 2007). This neglect may be explained by our attempt to make the model as simple as possible for (i) explicit account for several phases in a polymer nanocomposite leads to a substantial increase in number of adjustable parameters, which makes difficult predictions of the mechanical response, and (ii) a detailed analysis of deformations at interfaces and in inter-phases where relatively large deformations are observed (Kaushik et al. 2011; Li et al. 2011a, 2011b) requires application of a more sophisticated apparatus of continuum mechanics with finite strains.

### A.1 Kinematics of plastic deformations

To describe plastic flow in the equivalent medium at small strains, the strain tensor for macro-deformation $\hat{\epsilon}$ is presented as the sum of elastic strain tensor $\hat{\epsilon}_{\mathrm{e}}$ and plastic strain tensor $\hat{\epsilon}_{\mathrm{p}}$

$$\hat{\epsilon} = \hat{\epsilon}_{\mathrm{e}} + \hat{\epsilon}_{\mathrm{p}}. \tag{A.1}$$

With reference to conventional phenomenological models with two plastic elements connected in series, the plastic strain tensor $\hat{\epsilon}_{\mathrm{p}}$ is split into the sum of two components

$$\hat{\epsilon}_{\mathrm{p}} = \hat{\epsilon}_{\mathrm{p1}} + \hat{\epsilon}_{\mathrm{p2}}. \tag{A.2}$$

It is presumed that tensors $\hat{\epsilon}_{\mathrm{p1}}$ and $\hat{\epsilon}_{\mathrm{p2}}$ describe inelastic deformations in crystalline and amorphous phases, respectively. As no special phase is introduced for the analysis of deformation in stacks of clay platelets, the amorphous phase is associated with an ensemble of polymer chains in the rubbery state with randomly distributed nanoparticles.

The strain rate for plastic deformation in the crystalline phase is proportional to the strain rate for macro-deformation,

$$\frac{\mathrm{d}\hat{\epsilon}_{\mathrm{p1}}}{\mathrm{d}t} = \phi \frac{\mathrm{d}\hat{\epsilon}}{\mathrm{d}t}, \tag{A.3}$$

where the non-negative function $\phi$ (i) vanishes in the undeformed state (which means that no plastic deformation occurs at very small strains), (ii) monotonically grows under active loading and decreases under retraction (which reflects stress-induced acceleration of plastic flow), and (iii) reaches its ultimate value $\phi_\infty = 1$ at large strains (when the rates of plastic deformation and macro-deformation coincide). Changes in $\phi$ with time are governed by the differential equation

$$\frac{\mathrm{d}\phi}{\mathrm{d}t} = \pm a(1-\phi)^2 \dot{\epsilon}, \qquad \phi(0) = 0, \tag{A.4}$$

where the signs "+" and "−" correspond to loading and retraction, respectively, and

$$\dot{\epsilon} = \left( \frac{2}{3} \frac{\mathrm{d}\hat{\epsilon}}{\mathrm{d}t} : \frac{\mathrm{d}\hat{\epsilon}}{\mathrm{d}t} \right)^{\frac{1}{2}}$$

stands for the equivalent strain rate for macro-deformation. The coefficient $a$ adopts different values $a_1$ and $a_2$ under active deformation and unloading.

For uniaxial tensile cyclic deformation, which is the subject of this work, loading and unloading processes are determined unambiguously. For an arbitrary three-dimensional deformation, they can be defined following the approaches proposed by Bari and Hassan (2002) and Xia et al. (2005).

### A.2 Heterogeneity of the network

An inhomogeneous transient polymer network is composed of meso-domains with various activation energies for rearrangement of chains. The rate of separation of active chains from their junctions in a meso-domain with activation energy $u$ is governed by the Eyring equation $\Gamma = \gamma \exp[-u/(k_B T)]$, where $\gamma$ is an attempt rate, $k_B$ denotes Boltzmann's constant, and $T$ stands for the absolute temperature. Confining the analysis to isothermal processes and introducing dimensionless activation energy $v = u/(k_B T)$, we present this equation in the form

$$\Gamma(v) = \gamma \exp(-v). \tag{A.5}$$

Denote by $N$ concentration of active chains in the equivalent network (Tanaka and Edwards 1992). The number of active chains $n_0(v)$ in meso-domains with activation energy $v$ (per unit volume) reads

$$n_0(v) = N f(v), \tag{A.6}$$

where $f(v)$ stands for a distribution function of meso-domains. With reference to the random energy model (Derrida 1980), the quasi-Gaussian expression is adopted for this function

$$f(v) = f_0 \exp\left[-\frac{1}{2}\left(\frac{v}{\Sigma}\right)^2\right] \quad (v \geq 0), \qquad f(v) = 0 \quad (v < 0). \tag{A.7}$$

An advantage of (A.7) is that it involves the only adjustable parameter $\Sigma > 0$. The pre-factor $f_0$ is determined from the normalization condition $\int_0^\infty f(v)\,\mathrm{d}v = 1$. Parameters $N$, $\gamma$, and $\Sigma$ are assumed to be independent of mechanical factors.

### A.3 Rearrangement of chains

Rearrangement of a temporary network is described by a function $n(t, \tau, v)$ which equals the number (per unit volume) of temporary chains at time $t \geq 0$ that have returned into the active state before instant $\tau \leq t$ and belong to a meso-domain with energy $v$. The number of active chains in meso-domains with energy $v$ at time $t$ reads

$$n(t, t, v) = n_0(v), \tag{A.8}$$

while the number of chains that were active at the initial instant $t = 0$ and have not separated from their junctions until time $t$ is $n(t, 0, v)$. The number of chains that were active at the initial instant and detach from their junctions within the interval $[t, t + \mathrm{d}t]$ reads $-\partial n/\partial t\,(t, 0, v)\,\mathrm{d}t$, the number of dangling chains that return into the active state within the interval $[\tau, \tau + \mathrm{d}\tau]$ is given by $P(\tau, v)\mathrm{d}\tau$ with

$$P(\tau, v) = \frac{\partial n}{\partial \tau}(t, \tau, v)|_{t=\tau}, \tag{A.9}$$

and the number of chains that merged (for the last time) with the network within the interval $[\tau, \tau + \mathrm{d}\tau]$ and detach from their junctions within the interval $[t, t + \mathrm{d}t]$ equals $-\partial^2 n/\partial t \partial \tau(t, \tau, v)\,\mathrm{d}t\,\mathrm{d}\tau$. Detachment of chains from their junctions is described by the kinetic equations

$$\frac{\partial n}{\partial t}(t, 0, v) = -\Gamma(v) n(t, 0, v), \qquad \frac{\partial^2 n}{\partial t \partial \tau}(t, \tau, v) = -\Gamma(v)\frac{\partial n}{\partial \tau}(t, \tau, v), \tag{A.10}$$

which mean that the number of active chains separating from their junctions per unit time is proportional to the total number of active chains in an appropriate meso-domain. Integration of (A.10) with initial conditions (A.6), (A.8), and (A.9) implies that

$$n(t, 0, v) = N f(v) \exp\bigl[-\Gamma(v) t\bigr], \qquad \frac{\partial n}{\partial \tau}(t, \tau, v) = N f(v) \Gamma(v) \exp\bigl[-\Gamma(v)(t - \tau)\bigr]. \tag{A.11}$$

## A.4 Stress–strain relations

The strain energy of an active chain reads

$$w = \frac{1}{2}\bar{\mu}\hat{\epsilon}_{\mathrm{e}} : \hat{\epsilon}_{\mathrm{e}}, \tag{A.12}$$

where $\bar{\mu}$ stands for rigidity of a chain, and the colon denotes convolution of tensors. The strain energy of a chain that has last returned into the active state at instant $\tau < t$ is determined by (A.12), where $\hat{\epsilon}_{\mathrm{e}}(t)$ is replaced with $\hat{\epsilon}_{\mathrm{e}}(t) - \hat{\epsilon}_{\mathrm{e}}(\tau)$. The strain energy density (per unit volume) of individual chains in a transient polymer network is given by

$$W_1(t) = \frac{1}{2}\bar{\mu}\biggl[\int_0^\infty n(t, 0, v)\,\mathrm{d}v\,\hat{\epsilon}_{\mathrm{e}}(t) : \hat{\epsilon}_{\mathrm{e}}(t) + \int_0^\infty \mathrm{d}v \int_0^t \frac{\partial n}{\partial \tau}(t, \tau, v)\bigl(\hat{\epsilon}_{\mathrm{e}}(t) - \hat{\epsilon}_{\mathrm{e}}(\tau)\bigr) : \bigl(\hat{\epsilon}_{\mathrm{e}}(t) - \hat{\epsilon}_{\mathrm{e}}(\tau)\bigr)\,\mathrm{d}\tau\biggr]. \tag{A.13}$$

The first term in (A.13) equals the energy of active chains that have not been rearranged within the interval $[0, t]$. The other term expresses the energy of chains that have last merged with the network at various instants $\tau \in [0, t]$ and remained active until instant $t$.

The energy of interaction between chains in the equivalent network (per unit volume) is described by the formula similar to (A.12),

$$W_2 = \frac{1}{2}\tilde{\mu}\hat{\epsilon}_{\mathrm{p2}} : \hat{\epsilon}_{\mathrm{p2}}, \tag{A.14}$$

where $\tilde{\mu} > 0$ stands for an analog of elastic modulus, and $\hat{\epsilon}_{\mathrm{p2}}$ describes irreversible deformation in the amorphous phase. The function $W_2$ takes into account inter-chain interactions in the amorphous matrix and interactions between polymer chains and clay platelets and their stacks.

The strain energy density of the equivalent network equals the sum of strain energies of individual chains and the energy of interaction

$$W = W_1 + W_2. \tag{A.15}$$

Differentiation of (A.15) with respect to time with the use of (A.10), (A.13), and (A.14) results in

$$\frac{\mathrm{d}W}{\mathrm{d}t}(t)=\bar{\mu}\left[\int_0^\infty n(t,0,v)\,\mathrm{d}v\,\hat{\epsilon}_{\mathrm{e}}(t)+\int_0^\infty \mathrm{d}v\int_0^t \frac{\partial n}{\partial\tau}(t,\tau,v)\big(\hat{\epsilon}_{\mathrm{e}}(t)-\hat{\epsilon}_{\mathrm{e}}(\tau)\big)\,\mathrm{d}\tau\right]:\frac{\mathrm{d}\hat{\epsilon}_{\mathrm{e}}}{\mathrm{d}t}(t)$$
$$+\tilde{\mu}\hat{\epsilon}_{\mathrm{p2}}(t):\frac{\mathrm{d}\hat{\epsilon}_{\mathrm{p2}}}{\mathrm{d}t}(t)-J(t), \tag{A.16}$$

where

$$J(t)=\frac{1}{2}\bar{\mu}\int_0^\infty \Gamma(v)\,\mathrm{d}v\left[n(t,0,v)\,\hat{\epsilon}_{\mathrm{e}}(t):\hat{\epsilon}_{\mathrm{e}}(t)\int_0^t\frac{\partial n}{\partial\tau}(t,\tau,v)\big(\hat{\epsilon}_{\mathrm{e}}(t)-\hat{\epsilon}_{\mathrm{e}}(\tau)\big):\big(\hat{\epsilon}_{\mathrm{e}}(t)-\hat{\epsilon}_{\mathrm{e}}(\tau)\big)\,\mathrm{d}\tau\right]\geq 0.$$

Transformation of (A.16) by means of (A.1)–(A.3), (A.6), and (A.8) yields

$$\frac{\mathrm{d}W}{\mathrm{d}t}(t)=\bar{\mu}\left[N\hat{\epsilon}_{\mathrm{e}}(t)-\int_0^\infty \mathrm{d}v\int_0^t\frac{\partial n}{\partial\tau}(t,\tau,v)\hat{\epsilon}_{\mathrm{e}}(\tau)\,\mathrm{d}\tau\right]:\left[\big(1-\phi(t)\big)\frac{\mathrm{d}\hat{\epsilon}}{\mathrm{d}t}(t)-\frac{\mathrm{d}\hat{\epsilon}_{\mathrm{p2}}}{\mathrm{d}t}(t)\right]$$
$$+\tilde{\mu}\hat{\epsilon}_{\mathrm{p2}}(t):\frac{\mathrm{d}\hat{\epsilon}_{\mathrm{p2}}}{\mathrm{d}t}(t)-J(t). \tag{A.17}$$

For isothermal volume-preserving deformation, the Clausius–Duhem inequality reads

$$\frac{\mathrm{d}Q}{\mathrm{d}t}=-\frac{\mathrm{d}W}{\mathrm{d}t}+\hat{\sigma}':\frac{\mathrm{d}\hat{\epsilon}}{\mathrm{d}t}\geq 0, \tag{A.18}$$

where $Q$ stands for internal dissipation per unit volume, and $\hat{\sigma}'$ denotes the deviatoric part of the stress tensor $\hat{\sigma}$. Combining (A.17) and (A.18) and using (A.11), we arrive at the stress–strain relation

$$\hat{\sigma}(t)=-p(t)\hat{I}+\mu\big(1-\phi(t)\big)\left[\hat{\epsilon}_{\mathrm{e}}(t)-\int_0^\infty f(v)\,\mathrm{d}v\int_0^t\Gamma(v)\right.$$
$$\left.\times\exp\big(-\Gamma(v)(t-\tau)\big)\hat{\epsilon}_{\mathrm{e}}(\tau)\,\mathrm{d}\tau\right], \tag{A.19}$$

where $\mu=\bar{\mu}N$, $p$ is an unknown pressure, and $\hat{I}$ stands for the unit tensor.

It follows from (A.18) and (A.19) that

$$\frac{\mathrm{d}Q}{\mathrm{d}t}(t)=J(t)+\mu\left[\hat{\epsilon}_{\mathrm{e}}(t)-R\hat{\epsilon}_{\mathrm{p2}}(t)-\int_0^\infty f(v)\hat{Z}(t,v)\,\mathrm{d}v\right]:\frac{\mathrm{d}\hat{\epsilon}_{\mathrm{p2}}}{\mathrm{d}t}(t)\geq 0, \tag{A.20}$$

where $R$ adopts the values

$$R_1=\frac{\tilde{\mu}_1}{\mu},\qquad R_2=\frac{\tilde{\mu}_2}{\mu} \tag{A.21}$$

under loading and retraction, and

$$\hat{Z}(t,v)=\int_0^t\Gamma(v)\exp\big(-\Gamma(v)(t-\tau)\big)\hat{\epsilon}_{\mathrm{e}}(\tau)\,\mathrm{d}\tau. \tag{A.22}$$

Formula (A.22) implies that the function $\hat{Z}(t,v)$ is governed by the differential equation

$$\frac{\partial\hat{Z}}{\partial t}(t,v)=\Gamma(v)\big[\hat{\epsilon}_{\mathrm{e}}(t)-\hat{Z}(t,v)\big],\quad \hat{Z}(0,v)=0. \tag{A.23}$$

The Clausius–Duhem inequality (A.20) is satisfied provided that

$$\frac{\mathrm{d}\hat{\epsilon}_{\mathrm{p2}}}{\mathrm{d}t}(t)=S\dot{\epsilon}\left[\hat{\epsilon}_{\mathrm{e}}(t)-R\hat{\epsilon}_{\mathrm{p2}}(t)-\int_0^\infty f(v)\hat{Z}(t,v)\,\mathrm{d}v\right], \tag{A.24}$$

where the coefficient $S > 0$ adopts different values, $S_1$ and $S_2$, under loading and unloading [under condition (A.24), the last term in (A.20) becomes a positive-definite quadratic form].

Stress–strain relation (A.19) together with kinematic equations (A.1), (A.2) and kinetic equations (A.3), (A.4), (A.24) provide constitutive equations for the viscoelastoplastic behavior of polymer nanocomposites under cyclic deformation. These equations involve three material constants, $\mu$, $\gamma$, $\Sigma$, and six adjustable functions, $a_1$, $a_2$, $R_1$, $R_2$, $S_1$, $S_2$, with the following physical meaning:

- $\mu$ stands for an elastic modulus of a polymer nanocomposite,
- $\gamma$ and $\Sigma$ characterize its linear viscoelastic behavior,
- $a_1$ and $a_2$ describe irreversible deformation in the crystalline phase under loading and unloading,
- $R_1$, $S_1$ and $R_2$, $S_2$ characterize plastic flow in the amorphous matrix under active deformation and retraction.

## References


Ayoub, G., Zairi, F., Nait-Abdelaziz, M., Gloaguen, J.M.: Modelling large deformation behaviour under loading-unloading of semicrystalline polymers: Application to a high density polyethylene. Int. J. Plast. **26**, 329–347 (2010)

Ayoub, G., Zairi, F., Nait-Abdelaziz, M., Gloaguen, J.M.: Modeling the low-cycle fatigue behavior of visco-hyperelastic elastomeric materials using a new network alteration theory: Application to styrene-butadiene rubber. J. Mech. Phys. Solids **59**, 473–495 (2011)

Bari, S., Hassan, T.: An advancement in cyclic plasticity modeling for multiaxial ratcheting simulation. Int. J. Plast. **18**, 873–894 (2002)

Bikiaris, D.N., Papageorgiou, G.Z., Pavlidou, E., Vouroutzis, N., Palatzoglou, P., Karayannidis, G.P.: Preparation by melt mixing and characterization of isotactic polypropylene/$SiO_2$ nanocomposites containing untreated and surface-treated nanoparticles. J. Appl. Polym. Sci. **100**, 2684–2696 (2006)

Bouchart, V., Brieu, M., Bhatnagar, N., Kondo, D.: A multiscale approach of nonlinear composites under finite deformation: Experimental characterization and numerical modeling. Int. J. Solids Struct. **47**, 1737–1750 (2010)

Chaboche, J.L.: A review of some plasticity and viscoplasticity constitutive theories. Int. J. Plast. **24**, 1642–1693 (2008)

Cotterell, B., Chia, J.Y.H., Hbaieb, K.: Fracture mechanisms and fracture toughness in semicrystalline polymer nanocomposites. Eng. Fract. Mech. **74**, 1054–1078 (2007)

Derrida, B.: Random-energy model: limit of a family of disordered models. Phys. Rev. Lett. **45**, 79–92 (1980)

Drozdov, A.D.: Constitutive model for cyclic deformation of perfluoroelastomers. Mech. Time-Depend. Mater. **13**, 275–299 (2009)

Drozdov, A.D.: Cyclic viscoelastoplasticity and low-cycle fatigue of polymer composites. Int. J. Solids Struct. **48**, 2026–2040 (2011)

Drozdov, A.D., Christiansen, J.deC.: Cyclic viscoplasticity of high-density polyethylene: Experiments and modeling. Comput. Mater. Sci. **39**, 465–480 (2007)

Drozdov, A.D., Hog Lejre, A.-L., Christiansen, J.deC.: Viscoelasticity, viscoplasticity, and creep failure of polypropylene/clay nanocomposites. Compos. Sci. Technol. **69**, 2596–2603 (2009)

Drozdov, A.D., Christiansen, J.deC., Klitkou, R.: Volume growth and viscoplasticity of polymer/clay nanocomposites: experiments and modeling. Int. J. Appl. Math. Mech. **7**, 87–110 (2011)

Fu, S.-Y., Feng, X.-Q., Lauke, B., Mai, Y.-W.: Effects of particle size, particle/matrix interface adhesion and particle loading on mechanical properties of particulate polymer composites. Composites B **39**, 933–961 (2008)

Hsieh, A.J., Moy, P., Beyer, F.L., Madison, P., Napadensky, E., Ren, J., Krishnamoorti, R.: Mechanical response and rheological properties of polycarbonate layered-silicate nanocomposites. Polym. Eng. Sci. **44**, 825–837 (2004)

Jancar, J., Douglas, J.F., Starr, F.W., Kumar, S.K., Cassagnau, P., Lesser, A.J., Sternstein, S.S., Buehler, M.J.: Current issues in research on structure-property relationships in polymer nanocomposites. Polymer **51**, 3321–3343 (2010)

Kang, G.: Ratchetting: Recent progresses in phenomenon observation, constitutive modeling and application. Int. J. Fatigue **30**, 1448–1472 (2008)

Kaushik, A.K., Waas, A.M., Arruda, E.M.: A constitutive model for finite deformation response of layered polyurethane–montmorillonite nanocomposites. Mech. Mater. **43**, 186–193 (2011)
Li, Y., Waas, A.M., Arruda, E.M.: A closed-form, hierarchical, multi-interphase model for composites—Derivation, verification and application to nanocomposites. J. Mech. Phys. Solids **59**, 43–63 (2011a)
Li, Y., Waas, A.M., Arruda, E.M.: The effects of the interphase and strain gradients on the elasticity of layer by layer (LBL) polymer/clay nanocomposites. Int. J. Solids Struct. **48**, 1044–1053 (2011b)
Lietz, S., Yang, J.-L., Bosch, E., Sandler, J.K.W., Zhang, Z., Altstadt, V.: Improvement of the mechanical properties and creep resistance of SBS block copolymers by nanoclay filler. Macromol. Mater. Eng. **292**, 23–32 (2007)
Luo, J.-J., Daniel, I.M.: Characterization and modeling of mechanical behavior of polymer/clay nanocomposites. Compos. Sci. Technol. **63**, 1607–1616 (2003)
Mizuno, M., Sanomura, Y.: Phenomenological formulation of viscoplastic constitutive equation for polyethylene by taking into account strain recovery during unloading. Acta Mech. **207**, 83–93 (2009)
Mortezaei, M., Famili, M.H.N., Kokabi, M.: The role of interfacial interactions on the glass-transition and viscoelastic properties of silica/polystyrene nanocomposite. Compos. Sci. Technol. **71**, 1039–1045 (2011)
Pavlidou, S., Papaspyrides, C.D.: A review on polymer–layered silicate nanocomposites. Progr. Polym. Sci. **33**, 1119–1198 (2008)
Qiao, R., Brinson, L.C.: Simulation of interphase percolation and gradients in polymer nanocomposites. Compos. Sci. Technol. **69**, 491–499 (2009)
Rastogi, S., Lippits, D.R., Terry, A.E., Lemstra, P.J.: The role of the interphase on the chain mobility and melting of semi-crystalline polymers; A study on polyethylenes. Lect. Notes Phys. **714**, 285–327 (2007)
Sai, K.: Multi-mechanism models: Present state and future trends. Int. J. Plast. **27**, 250–281 (2011)
Sheng, N., Boyce, M.C., Parks, D.M., Rutledge, G.C., Abes, J.I., Cohen, R.E.: Multiscale micromechanical modeling of polymer/clay nanocomposites and the effective clay particle. Polymer **45**, 487–506 (2004)
Su, F.-H., Yan, J.-H., Huang, H.-X.: Structure and melt rheology of long-chain branching polypropylene/clay nanocomposites. J. Appl. Polym. Sci. **119**, 1230–1238 (2011)
Sullivan, R.W.: Development of a viscoelastic continuum damage model for cyclic loading. Mech. Time-Depend. Mater. **12**, 329–342 (2008)
Tanaka, F., Edwards, S.F.: Viscoelastic properties of physically cross-linked networks. Transient network theory. Macromolecules **25**, 1516–1523 (1992)
Tjong, S.C.: Structural and mechanical properties of polymer nanocomposites. Mater. Sci. Eng. R **53**, 73–197 (2006)
Wang, K., Liang, S., Deng, J., Yang, H., Zhang, Q., Fu, Q., Dong, X., Wang, D., Han, C.C.: The role of clay network on macromolecular chain mobility and relaxation in isotactic polypropylene/organoclay nanocomposites. Polymer **47**, 7131–7144 (2006)
Wang, Z.D., Zhao, X.X.: Modeling and characterization of viscoelasticity of PI/$SiO_2$ nanocomposite films under constant and fatigue loading. Mater. Sci. Eng. A **486**, 517–527 (2008a)
Wang, Z.D., Zhao, X.X.: Creep resistance of PI/$SiO_2$ hybrid thin films under constant and fatigue loading. Composites A **39**, 439–447 (2008b)
Xia, Z., Shen, X., Ellyin, F.: An assessment of nonlinearly viscoelastic constitutive models for cyclic loading: The effect of a general loading/unloading rule. Mech. Time-Depend. Mater. **9**, 281–300 (2005)
Yakimets, I., Lai, D., Guigon, M.: Model to predict the viscoelastic response of a semi-crystalline polymer under complex cyclic mechanical loading and unloading conditions. Mech. Time-Depend. Mater. **11**, 47–60 (2007)
Yang, J.-L., Zhang, Z., Schlarb, A.K., Friedrich, K.: On the characterization of tensile creep resistance of polyamide 66 nanocomposites. Part I. Experimental results and general discussions. Polymer **47**, 2791–2801 (2006)
Zeng, Q.H., Yu, A.B., Lu, G.Q.: Multiscale modeling and simulation of polymer nanocomposites. Progr. Polym. Sci. **33**, 191–269 (2008)
Zhang, X., Loo, L.S.: Study of glass transition and reinforcement mechanism in polymer/layered silicate nanocomposites. Macromolecules **42**, 5196–5207 (2009)